Chapter 11
The Sept Iles Intrusive Suite, Quebec, Canada

Olivier Namur, Michael D. Higgins and Jacqueline Vander Auwera

Abstract The Sept Iles Intrusive Suite (Quebec, Canada) is made up of a large layered intrusion, late gabbro intrusions and a composite sill (Pointe du Criard Sill). The layered intrusion crystallized from a ferrobasaltic magma and is subdivided into a Layered Series of troctolite and gabbro, an anorthositic Upper Border Series and a granitic Upper Series. The formation of the Upper Border Series resulted from plagioclase flotation from the base to the roof of the magma chamber. Fractionation of troctolites and gabbros in the Layered Series resulted in SiO_2-enrichment and FeO_t-depletion of the residual melt, ultimately forming the granite of the Upper Series. The solidification history of the Layered Series was interrupted by two major and a series of minor influxes of ferrobasaltic melt, significantly enlarging the size of the initial magma chamber. As a consequence, the Layered Series can be subdivided into three megacyclic units (MCU I, II and III). Mixing between resident magma and undifferentiated melt during replenishments had an important influence on both mineral compositions and the liquid lines of descent during the crystallization of the various megacyclic units. It is shown that the liquid line of descent during crystallization of MCU II reached silicate liquid immiscibility. Immiscible melts crystallized two different types of apatite-bearing gabbros, one of which is a major P–Ti–Fe deposit. Cumulate rocks in the layered intrusion show a wide range of crystallized interstitial liquid content. Expelling of this liquid from the crystal mush during solidification is explained both by compaction and compositional convection, but the relative efficiency of these two processes is shown to change significantly with differentiation.

O. Namur (✉)
Institute of Mineralogy, University of Hannover, 30167 Hannover, Germany
e-mail: o.namur@mineralogie.uni-hannover.de

M. D. Higgins
Sciences de la Terre, Université du Québec à Chicoutimi, 555 Blvd de l'université, Chicoutimi, Quebec G7H 2B1, Canada
e-mail: mhiggins@uqac.ca

J. Vander Auwera
Department of Geology, University of Liege, Liege, Belgium
e-mail: jvdauwera@ulg.ac.be

B. Charlier et al. (eds.), *Layered Intrusions,* Springer Geology,
DOI 10.1007/978-94-017-9652-1_11

Keywords Ferrobasalt · Cumulate · Anorthosite · Granite · Magma chamber processes

Introduction

The Sept Iles intrusive suite (Quebec, Canada) is made up of a layered intrusion, some 80 km in diameter, a series of late gabbro intrusions and the Pointe du Criard composite sill. This magmatic event occurred during the later part of the Ediacarian period (564 Ma; Higgins and van Breemen 1998) and played an important role in the evolution of the Precambrian continental crust of Laurentia. The layered intrusion, estimated to be the third largest in the world (Namur et al. 2010), comprises a lower Layered Series with troctolite and gabbro, an anorthositic Upper Border Series and a granitic Upper Series. According to Higgins (2005), all parts of the layered intrusion are comagmatic and related by fractional crystallization and other physical processes that occurred during solidification of the magma chamber.

Rocks from the Layered Series of the layered intrusion are dominated by plagioclase, olivine, clinopyroxene, Fe–Ti oxide minerals and apatite. They resulted from the crystallization of a ferrobasaltic melt (Namur et al. 2010) and strongly resemble the ferrogabbros of the Skaergaard intrusion (McBirney 1989), and the Upper Zone of the Bushveld Complex (Tegner et al. 2006). This troctolite-gabbro succession contains more than 20 cm- to m-thick layers enriched in magnetite and ilmenite, similar to those observed in the Bushveld complex (Cawthorn and Ashwal 2009). It also contains many dm-m blocks of anorthosite, somewhat similar to those observed in the Layered Series of the Skaergaard intrusion (Irvine et al. 1998; Higgins 2005). Mineral compositions in the Layered Series evolve upwards but the main trend is interrupted by two large and several small regressions to more primitive compositions. The most evolved rocks of the Layered Series are made up of apatite-bearing olivine gabbros which represent an important Fe–Ti–P deposit. The uppermost part of the Layered Series does not crop out but is thought to be structurally overlain by a 200–500 m-thick layer of anorthosite, locally containing cm- to m-scale pockets of syenitic to granitic material. Continuous outcrops in the southern part of the Sept Iles archipelago show that the anorthosite is overlain by km-scale cupolas of syenite and granite of two types: the first one contains abundant magmatic mafic enclaves and the second one is free of any enclaves.

Here we present an overview of the present understanding of the origin and evolution of the Sept Iles Intrusive Suite. We describe the different units of the Intrusive Suite with major focus on the layered intrusion. We present the stratigraphic evolution of rocks and mineral compositions in the layered intrusion and use them to describe how the magma chamber was filled and replenished. We also present field relationships and compositional data for rocks of the Sept Iles chilled margin, dykes cutting the Layered Series and silicic rocks from the Upper

Series that we use to determine the liquid line of descent of the layered intrusion and potential implications for other ferrobasaltic intrusions. We then show how the liquid line of descent controls some specific magma chamber processes such as plagioclase flotation, resulting in the formation of anorthosite at the roof of the magma chamber, and the expelling and/or exchange of interstitial melt from the crystal matrix during solidification. We finally describe how a silicate-liquid immiscibility process exerted a control on the Sept Iles liquid line of descent and how it contributed to the formation of large-scale Fe–Ti–P ore deposits.

Geological Setting

Regional Geology

The Sept Iles intrusive Suite (SIIS) is located on the north shore of the St Lawrence River, about 500 km to the north-east of Quebec City, Canada. It is a non-deformed and non-metamorphosed magmatic body emplaced into high-grade gneisses (Higgins 2005) of the allochthonous polycyclic belt of the Grenville geological province (Rivers et al. 1989; Rivers 2008). The age of the SIIS was originally determined from Rb–Sr isochrons on granite and syenite that gave results ranging from 538 ± 17 to 555 ± 2 Ma, with an average of ca. 540 Ma (Higgins and Doig 1977, 1981). The SIIS was re-dated at 564 ± 4 Ma using the U–Pb method on zircons extracted from a granophyre pod in the gabbroic cumulates (Higgins and van Breemen 1998). This age coincides with a large magmatic event in Eastern Laurentia, dominated by volcanic rocks (basalts) and plutons (alkaline plutons, carbonatites and kimberlites; Doig and Barton 1968; Doig 1970; Kamo et al. 1989; Kumarapeli 1993; Higgins and van Breemen 1998). This magmatic event, including the SIIS, was attributed to the initiation of the St Lawrence rift system during the opening of the Iapetus Ocean (Kumarapeli and Saull 1966). Given the large volume of magma represented in the SIIS, it is suggested that it might be related to a mantle plume (Hill et al. 1992; Higgins and van Breemen 1998), although the location of the SIIS on a major lithospheric discontinuity suggests that it may also result from lithospheric re-organization (Namur et al. 2010). In any case, the Sr isotopic composition of bulk-rocks and mineral separates from the SIIS implies a mantle source (Higgins and Doig 1981; Namur et al. 2010).

Higgins (2005) proposed that magmatic activity in the Sept Iles region started with the eruption of an unknown volume of flood basalts and that the SIIS was subsequently emplaced at the unconformity between the lavas and the Grenville basement rocks. No flood basalts are preserved anywhere in the Sept Iles area, but flood basalts commonly erupt during continental rifting, such as the opening of the St Lawrence rift system. Basalts of similar age to the SIIS are present to the southwest of Sept Iles (the Tibbit Hill Formation) and elsewhere in the Appalachians (Higgins and van Breemen 1998).

The Sept Iles Intrusive Suite

The SIIS is dinner-plate shaped, with a diameter of about 80 km and a maximum thickness of 7 km. Only 10 % crops out on the mainland and on the islands of the Sept Iles archipelago (Fig. 11.1). The quality of outcrops is relatively poor on the mainland, with the exception of rare quarries and along a power line crossing the SIIS from west to east. In contrast, outstanding outcrops of anorthosite, syenite and granite occur on the Marconi Peninsula and on the islands of the archipelago. These outcrops were therefore the first to be investigated and the SIIS was first described as an anorthosite massif (Higgins and Doig 1977, 1981) similar to Proterozoic massif-type anorthosites. However, unpublished mapping by T. Ahmedali in the 1960s and T. Feininger in 1985–1990 followed by detailed mapping by Cimon (1998) and geophysical studies by Loncarevic et al. (1990) have revealed that the mainland outcrops are more complicated than previously thought and expose a sequence of massive troctolites and layered gabbros that are overlain by anorthosite, syenite and granite. In light of these new data, the SIIS was then described as a single layered intrusion (Higgins and Doig 1986; Higgins 1991). However, a recent reinvestigation by Higgins (2005) suggests that the igneous activity around Sept Iles was more complex and that the Sept Iles intrusive rocks are better described as an intrusive suite (Sept Iles Intrusive Suite) of three magmatic components: a layered intrusion, the Pointe du Criard composite sill and a series of late-stage gabbros.

The Sept Iles Layered Intrusion

General Overview

The Sept Iles layered intrusion is by far the most voluminous unit of the SIIS although the relative volumes of the different units, including the layered intrusion, are not precisely known. Its size is well defined by a gravity anomaly, some 80 km in diameter, with a maximum Bouguer anomaly of 80 mGal, which is the largest gravity anomaly in eastern North America (Loncarevic et al. 1990). The layered intrusion is also defined by an important magnetic anomaly (Fig. 11.2). There is no evidence that the roof of the intrusion is still preserved. As proposed for other layered intrusions (e.g. the Bushveld Complex; Cheney and Twist 1991) it has been suggested that the initial intrusion was a sill and that subsidence of the floor due to the weight of the cumulate rocks is responsible for its final lopolithic form (Higgins 2005). Interest in the Sept Iles layered intrusion increased at the end of the 1980s because the composition and size of the intrusion suggested that it might host significant Ni, Cu and PGE resources. Three cores (DC-84670, 450 m; DC-84698 (DC-8), 1920 m and DC-84699 (DC-9), 2550 m), currently kept at the Ministère des Ressources Naturelles et de la Faune du Québec, were drilled in

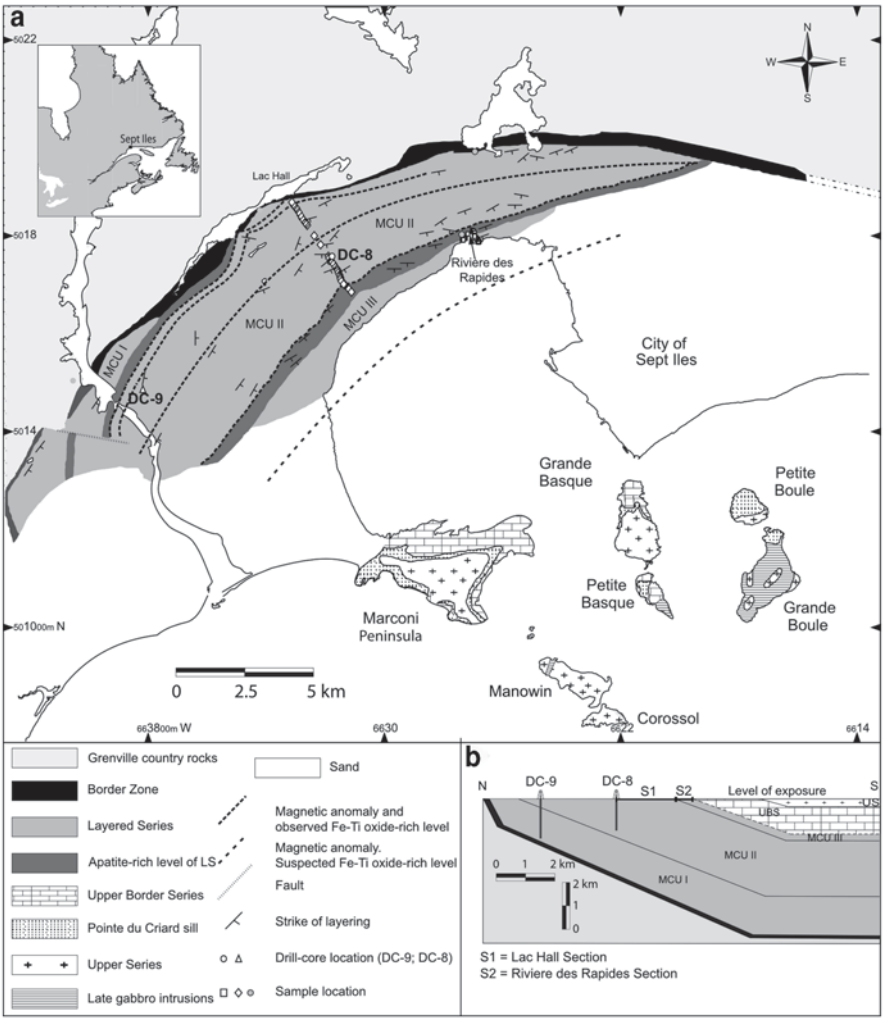

Fig. 11.1 **a** Geological map of the Sept Iles Intrusive Suite adapted from Higgins and Doig (1986) and Higgins (2005). Note the vertical and lateral subdivision of the Layered Series of the layered intrusion into three megacyclic units (*MCUI-III*). The inset map in the *upper left* corner shows the location of the map area in southeastern part of Canada. Locations of surface samples and drill-cores (*DC-8*; *DC-9*) from the Layered Series (Namur et al. 2010) are shown for reference. Detailed stratigraphic relationships between these samples can be seen in Figs 11.1b and 11.5. **b** Schematic cross-section of the Sept Iles layered intrusion. Note the vertical succession of the 3 MCUs of the Layered Series and the Upper Border Series and Upper Series. Note also the stratigraphic intervals intersected by the drill cores and where field samples were collected. *LS* Layered Series, *UBS* Upper Border Series, *US* Upper Series

the 1990s by Inco Inc (see location of DC-8 and DC-9 in Fig. 11.1) but no metallic ores were found. However, a 200 m thick sequence of apatite-bearing gabbro was discovered in DC-84699, while another interval, some 250 m in thickness,

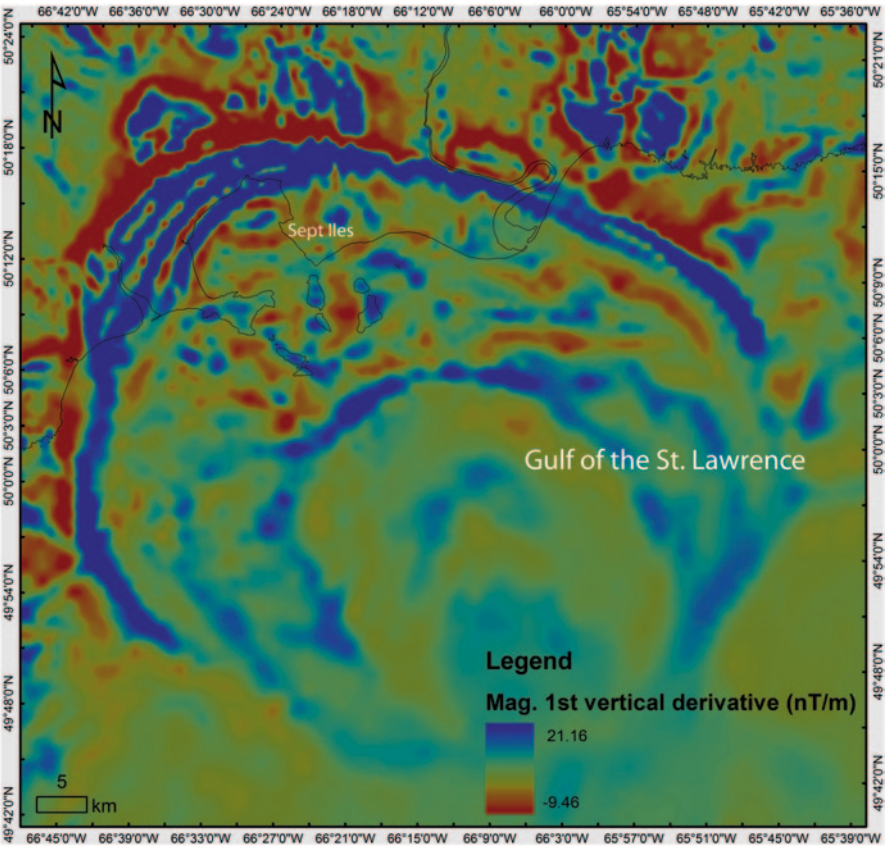

Fig. 11.2 Magnetic vertical gradient map of the Sept Iles area showing the Sept Iles layered intrusion and the country rocks to the north (1st vertical derivative in nT/m, resolution: 1 km) (data source: Natural Resources Canada). The Sept Iles layered intrusion is characterized by relatively high magnetic gradient compared to the country rocks. Curved east-west *blue bands* highlight the largest Fe–Ti oxide layers of the Sept Iles Layered Series. This map also highlights the size and circular shape of the layered intrusion. (Courtesy of Lajeunesse et al. (2013), Laval University, Quebec, Canada)

was known to occur on the mainland. The latter level, generally called the Critical Zone, was investigated at the end of the 1990s by the Soquem Inc. which drilled 30 cores 100–250 m long.

Using samples from the Inco drill-cores (see their stratigraphic distribution below) together with additional samples collected in the field, the Sept Iles layered intrusion was subdivided by Cimon (1998) into four series: a Lower Series dominated by massive troctolite, a Layered Series comprising layered gabbro, a Transitional Series made up of anorthosite and an Upper Series dominated by granite and minor syenite. However, more recent investigations by Higgins (2005) and Namur et al. (2010) along with comparisons with the Skaergaard intrusion have shown that the subdivision proposed by Cimon (1998) is inconsistent with the processes that

occurred during crystallization (see below). A simpler subdivision into the gabbro-troctolite Layered Series, the anorthositic Upper Border Series and the granite-syenite Upper Series has therefore been adopted (Fig. 11.1). It should already be noted that in contrast to the Skaergaard intrusion, the Upper Border Series does not correspond to a mirror image of the Layered Series but to a 200–500 m-thick unit dominated by anorthosite. However, the anorthosite may have served as a nucleation site for minor *in situ* crystallization of troctolite and gabbro at the roof of the chamber.

No continuity in drill-cores or in the field is observed between the Layered Series and the Upper Border Series. However, the presence of blocks of anorthosite in the Layered Series which are petrographically and compositionally identical to the anorthosite observed in the Upper Border Series suggests a genetic link between these two series. This is also confirmed by the presence of abundant syenite-granite pods in the anorthosite of the Upper Border Series that resemble the granophyre pockets observed in the most evolved cumulates of the Layered Series (Higgins and Doig 1981; Namur et al. 2010, 2011a). Continuous outcrops on the Marconi Peninsula and several islands show a vertical relationship between the anorthosite of the Upper Border Series and the syenite-granite of the Upper Border Series. These field relationships all together strongly suggest that the Layered Series, Upper Border Series and Upper Series all belong to the same intrusive body and are genetically related by a single process of crystallization in the Sept Iles magma chamber.

To the north, the Sept Iles layered intrusion is surrounded by a thin zone of massive fine-grained dolerite called the Sept Iles Border Zone. Geophysical data are not sufficiently detailed to determine whether it continues beneath the sea or if it only occurs in the north. Based on bulk-rock and mineral compositions, Cimon (1998) interpreted this unit as a separate intrusive body, younger in age than the Sept Iles layered intrusion and having crystallized from a more evolved parental magma. However, by analogy with other layered intrusions, this zone might also correspond to a chilled margin representing rapidly cooled magma against cold country rocks (Wager and Brown 1968; Hoover 1989) or to a marginal reversal made up of fine-grained cumulate rocks becoming increasingly more primitive upwards in the stratigraphy (Egorova and Latypov 2012).

The Sept Iles Border Zone

The exposed part of the Sept Iles layered intrusion is surrounded by a Border Zone (at least 20 m thick) of massive fine-grained dolerite with minor amounts of medium-grained monzonite, representing an abrupt contrast with the coarse-grained gabbros of the Layered Series and the highly deformed host Grenvillian gneisses (Fig. 11.1). The most external part of this zone contains abundant pods and lenses of evolved material, probably resulting from the local partial melting of the country rocks. It also contains abundant cm- to m-scale angular blocks of Grenvillian gneiss

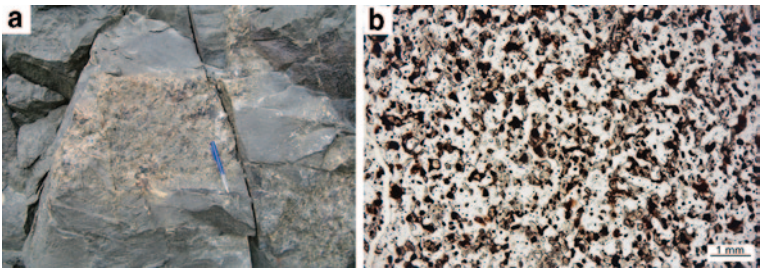

Fig. 11.3 **a** Photograph of fine-grained dolerite of the Sept Iles Border Zone. A dm-scale block of quartzite derived from the Grenvillian country rocks is included into the dolerite. Sept Iles mainland, looking north. **b** Photomicrograph of fine-grained dolerite from the Sept Iles Border Zone, dominated by plagioclase, clinopyroxene and Fe–Ti oxides. Transmitted light

(Fig. 11.3a). Dolerite from the Border Zone has granular texture and an average plagioclase size of 0.1–0.5 mm (Fig. 11.3b). It is dominated by lath-shaped, strongly zoned, locally antiperthitic, plagioclase, anhedral to subhedral clinopyroxene and anhedral Fe–Ti oxide patches dominated by magnetite (Fig. 11.3b). Anhedral to slightly rounded olivine and orthopyroxene are observed in some samples, together with minor needles of apatite (up to 300 μm long), and composite biotite-amphibole rims around clinopyroxene and Fe–Ti oxides. Traces of quartz, alkali-feldspar and zircon are observed in some samples. The monzonite is quite similar, except that it contains more quartz, amphibole and alkali-feldspar and less Fe–Ti oxides than the dolerite.

The Layered Series

Field Relationships, Modal Layering and Ore Deposits

From its contact with the Border Zone to the central part of the Layered Series, four main rock types have been recognized in the field: troctolite (Fig. 11.4a), Fe–Ti oxide-bearing troctolite, gabbro (Fig. 11.4b) and apatite-bearing gabbro. Troctolites and Fe–Ti oxide troctolites are coarse-grained massive rocks, while gabbros are finer-grained and exhibit mineral lamination. Igneous layering is commonly observed in gabbros (Fig. 11.4b), dipping 15–30 towards the centre of the intrusion, and showing a regular alternation of cm- to dm-thick mafic and more felsic layers. Layers commonly exhibit modal grading from olivine, pyroxene, ilmenite or magnetite-rich bases to plagioclase-rich tops. Modally-layered intervals locally with slump to trough structures and minor unconformities are especially evident in Fe–Ti oxide-rich gabbros. Most layers are ca. 10 cm-thick but may range from a few cm to more than 1 m. As described below, some Fe–Ti oxide-rich layers are however locally thicker than 15 m (Fig. 11.4c; Namur et al. 2010). Centimeter- to

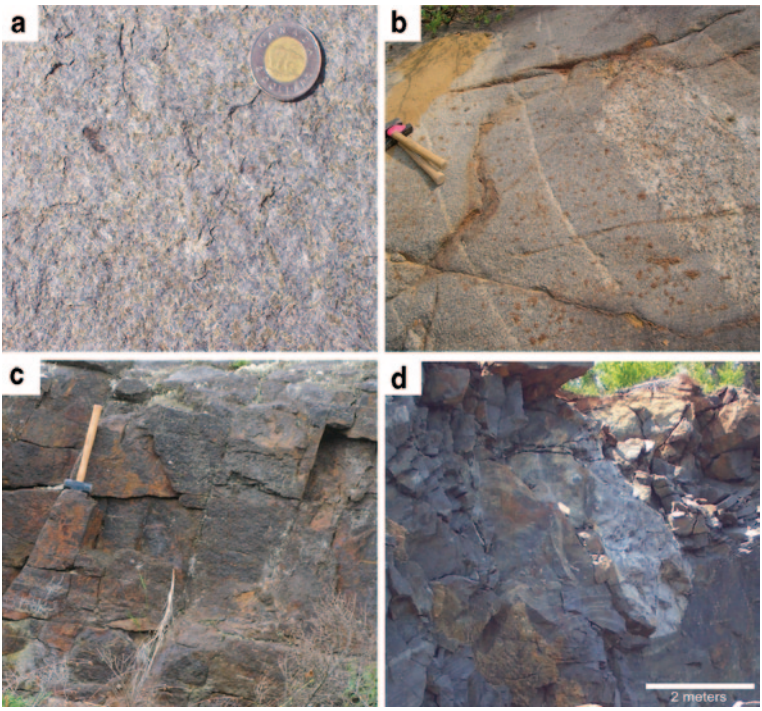

Fig. 11.4 Photographs of field relationships in the Layered Series. **a** Coarse-grained troctolite from MCU III, Rivière des Rapides. **b** Centimeter to decimeter thick rhythmic layering in gabbro showing alternating plagioclase-rich leucocratic layers and mafic mineral-rich melanocratic layers. To the *right* there is an autolith of pale anorthosite. Hall lake section. **c** Representative outcrop of a meter-thick massive Fe–Ti oxide layer, Sept Iles mainland. **d** Anorthositic autolith block within gabbros of the Layered Series. Note the deformation of the layering at the base of the autolith, suggesting that the block has foundered into a partially solid crystal pile, Sept Iles mainland

meter-scale blocks of anorthosite are abundant in the gabbro and locally deform the layering of the underlying rocks (Fig. 11.4b, d). They are especially abundant in gabbros from the western side of the intrusion.

Fe–Ti oxide mineralization is an important feature of the Sept Iles layered intrusion and occurs either as tabular or lens-shaped massive bodies. Tabular ore bodies are isomodal layers, 5 cm- to 15 m-thick (Fig. 11.4c), dominated by magnetite and ilmenite, concordant with the general layering, which have sharp lower and diffuse upper contacts.

Two ca. 200 m-thick apatite-rich gabbro units occur in the lower and middle part of the Layered Series. The lower unit is comprised of homogeneous leucocratic gabbro with 2–5 vol.% apatite, while the upper unit shows an alternation of melanocratic layers dominated by Fe–Ti oxides and apatite and plagioclase-rich layers (with very minor Fe–Ti oxides) on a scale of 1–20 m (Charlier et al. 2011; Namur et al. 2012a).

Subdivision of the Layered Series and Lithological Stratigraphy

The presence of two units of apatite-bearing gabbro and the disappearance of cumulus apatite at certain levels suggest that the fractionation trend of the Sept Iles parent magma was temporarily interrupted. This allowed the Layered Series to be subdivided into three megacyclic units (MCUs; Irvine 1982) with repeated characteristic sequences of cumulates (Namur et al. 2010). MCU I (1785 m-thick) and MCU II (2533 m-thick) are topped by apatite-bearing gabbro units (Fig. 11.5). MCU III is at least 396 m-thick, but its upper part is not exposed. The Layered Series is at least 4800 m thick (from −4210 to 549 m, with the 0 m reference level corresponding to the appearance of cumulus apatite in MCU II; Namur et al. 2010).

MCU I is characterized by the following succession of rocks: troctolite (plagioclase, olivine; po-C; notation following Irvine 1982), Fe–Ti oxide-troctolite (+ magnetite and ilmenite; pomi-C), gabbro (+ clinopyroxene; pomic-C), olivine-free gabbro (- olivine; pmic-C) and apatite-bearing olivine gabbro (+ olivine and apatite; pomica-C; Fig. 11.5). These units show contrasting mineral (see below) and bulk-rock compositions (Tables 11.1, 11.2). Troctolite (Fig. 11.6a) consists of plagioclase (ca. 70 vol.%) and olivine (ca. 30 vol.%), with minor clinopyroxene, Fe–Ti oxides and apatite. It has been shown by Namur et al. (2011a) that some plagioclase is missing as compared to theoretical cotectic proportions and that olivine is therefore in excess. Fe–Ti oxide-troctolite (Fig. 11.6b) is identical to troctolite except that the proportion of Fe–Ti oxides is significantly higher (10–15 vol.%). The latter minerals form large anhedral grains (up to 10 mm), frequently polycrystalline and generally dominated by magnetite. Olivine gabbro, gabbro (Fig. 11.6c) and apatite-bearing olivine gabbro (or locally nelsonite; Fig. 11.6d) are medium grained (1–4 mm) with plagioclase and clinopyroxene generally defining a strong lamination.

MCU II consists of a complex succession of Fe–Ti oxide-troctolite (pomi-C), olivine gabbro (pomic-C) and gabbro (pmic-C), topped by a 200 m-thick unit of apatite-bearing olivine gabbro (pomica-C). Olivine is relatively abundant in the lower part of MCU II but tends to decrease upwards. It is very low (less than 10 vol.%) in two intervals (pmic-C) where olivine is interpreted as an intercumulus phase (Fig. 11.5). The mode of clinopyroxene is highly variable in the lowest 1300 m of MCU II, where this mineral alternates between cumulus and interstitial on a scale of ca. 100 m. The amount of clinopyroxene then becomes more uniform and higher (ca. 30 vol.%) towards the top of MCU II.

In MCU III, clinopyroxene and apatite are minor minerals and the rocks are therefore predominantly Fe–Ti oxide-troctolite (pomi-C) and troctolite (po-C). The upper part of MCU III is not exposed (Fig. 11.5).

Cryptic Layering

The base of MCU I displays a 60 m-thick basal reversal in the composition of plagioclase (An_{63-68}; An=[Ca/(Ca+Na]), olivine (Fo_{68-74}; Fo=[Mg/(Mg+Fe^{2+}]) and clinopyroxene ($Mg\#_{76-79}$; Mg#=[Mg/(Mg+Fe^{2+}]), followed by a continuous decrease of

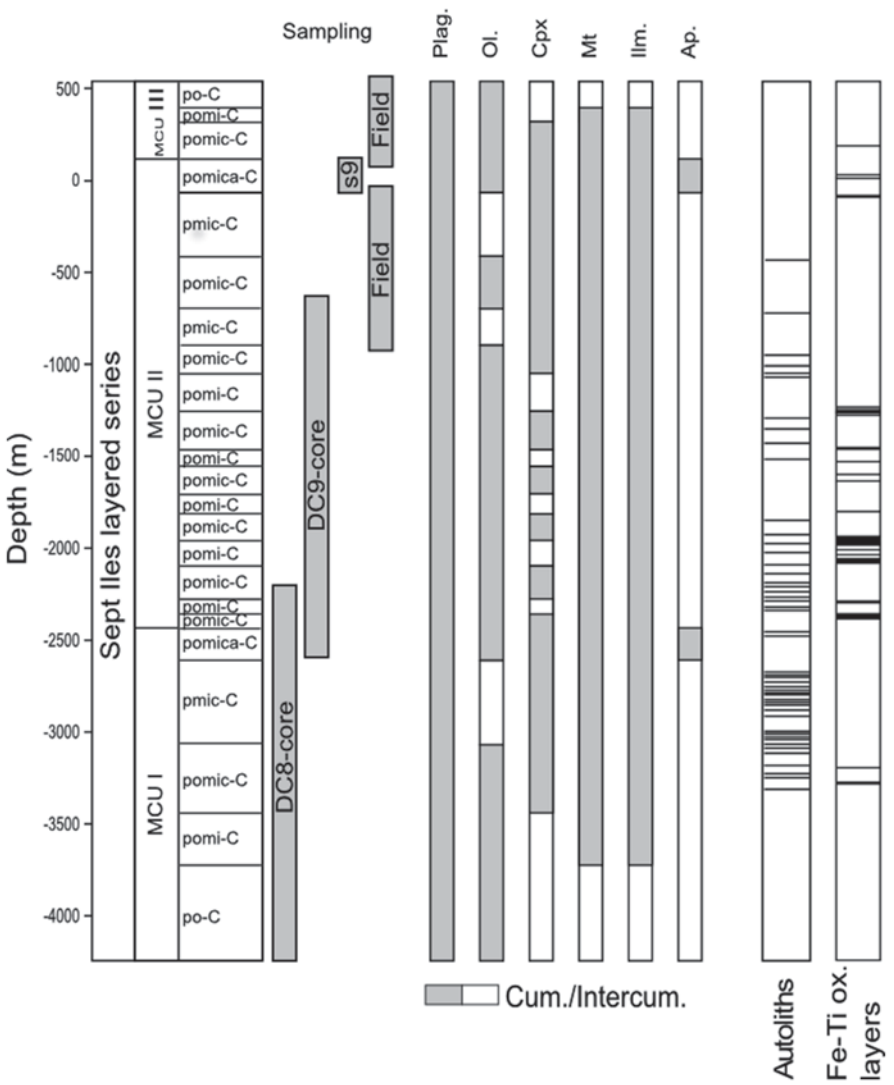

Fig. 11.5 Stratigraphy of the Sept Iles Layered Series as it crops out on the mainland and as intersected by the drill cores. The subdivision into three megacyclic units (*MCUI-III*) is shown. The stratigraphic intervals intersected by the drill cores are shown for reference together with the stratigraphic intervals where field samples were collected. The distribution of cumulus (*grey*) and intercumulus (*white*) assemblages is also shown and was determined based on geochemical constraints and mineral modes (see text for details). Classification of cumulus assemblages following Irvine (1982): *p* plagioclase, *o* olivine, *m* magnetite, *i* ilmenite, *c* clinopyroxene, *a* apatite, *-C* cumulate. The distribution of the main anorthosite blocks (autoliths; see details in the text for their origin) and Fe–Ti oxide layers is also shown. The '0-meter' reference level corresponds to the first appearance of cumulus apatite in MCU II

Table 11.1 Mineral assemblages and mineral compositions in the Sept Iles Layered Series. (Data from Namur et al. (2010); cumulate classification following Irvine (1982))

		Average mineral proportions (wt.%)						Range of silicate mineral compositions			Isotop. Comp.
Unit	Thickness (m)	Plagioclase	Olivine	Magnetite	Ilmenite	Cpx	Apatite	Plag (An%)	Olivine (Fo%)	Cpx ($Mg^{\#}$%)	$(^{87}Sr/^{86}Sr)_{564}$
MCU I											
po-C	522	67	33	–	–	–	–	68–61	73–66	–	0.70372–0.70392
pomi-C	340	53	25	13	9	–	–	61–60	66–66	–	0.70376
pomic-C	326	47	12	12	10	19	–	60–57	66–65	75–73	0.70382
pmic-C	432	47	–	13	12	28	–	57–51		74–71	0.70382
pomica-C	165	47	21	9	6	12	5	51–47	60–55	71–68	0.70393–0.70405
MCU II											
pomi-C	543	56	20	17	7	–	–	62–60	70–68	–	0.70381–0.70389
pomic-C	1116	47	14	13	9	17	–	60–56	68–64	76–73	0.70444
pmic-C	722	46	–	14	11	29		56–52		74–70	0.70396–0.70462
pomica-C	171	43	19	12	6	14	6	52–34	57–21	70–57	0.70493
MCU III											
po-C	132	68	32	–	–	–	–	69–62	71–65	–	0.70360
pomi-C	120	56	27	12	8	–	–	62–60	67–65	–	0.70382–0.70383
pomic-C	144	52	12	14	7	15	–	60–39	65–45	76–66	–

p plagioclase, *o* olivine, *m* magnetite, *i* ilmenite, *c* clinopyroxene, *a* apatite

Table 11.2 Average bulk rock compositions of cumulus units in the Layered Series (MCU I). (Data from Namur et al. (2010))

Unit	po-C	pomi-C	pomic-C	pmic-C	pomica-C
SiO_2 (wt.%)	45.23	40.03	41.08	40.04	39.90
TiO_2	0.58	3.87	4.70	6.75	4.45
Al_2O_3	20.87	18.24	16.05	14.01	14.69
FeO_t	8.26	18.32	17.47	18.95	17.22
MnO	0.11	0.16	0.17	0.20	0.26
MgO	8.71	7.73	7.50	6.44	6.50
CaO	9.75	8.47	10.07	10.97	10.89
Na_2O	2.58	2.57	2.58	2.48	3.01
K_2O	0.23	0.21	0.17	0.16	0.24
P_2O_5	0.06	0.04	0.04	0.05	2.39
LOI	0.15	0.28	0.15	0.04	0.20
Total	99.86	99.90	99.99	100.09	99.74

these parameters to the top of MCU I, where they reach An_{47}, Fo_{55} and cpx-$Mg\#_{68}$ (Fig. 11.7). The major element compositions of magnetite and ilmenite do not show any clear evolution throughout MCU I. In contrast, the Cr-content of magnetite first increases in po-C rocks (from the base of MCU I to −3600 m), where it reaches 10,000 ppm, before dropping quickly below the XRF detection limit (e.g. 5 ppm, Duchesne and Bologne 2009) after the appearance of cumulus Fe–Ti oxides. MCU II starts with a rapid, progressive, upwards increase in the An-content of plagioclase (An_{47} to An_{64}), Fo-content of olivine (Fo_{55} to Fo_{72}) and Mg# of clinopyroxene ($Mg\#_{68}$ to $Mg\#_{78}$). Mineral compositions (ca. An_{62}; Fo_{70}; cpx-$Mg\#_{75}$) are then relatively constant to −590 m. The upper part of MCU II then shows a continuous evolution of minerals down to An_{34}, Fo_{21} and cpx-$Mg\#_{55}$ at the top of the megacyclic unit. The magnetite Cr-content drops rapidly below the XRF detection limit in this upper section. In MCU III, the compositions of silicate minerals show a significant, progressive regression to An_{70}, Fo_{75} and cpx-$Mg\#_{78}$. The Cr-content of magnetite also increases to 23,000 ppm at the top of the exposed MCU III.

Sr-isotope ratios $(^{87}Sr/^{86}Sr)_{564}$ in plagioclase separates from the Sept Iles Layered Series vary between 0.70360 and 0.70498. This ratio increases upwards in each MCU and its evolution is strongly anti-correlated with the evolution of plagioclase-An, olivine-Fo and clinopyroxene-Mg#. The highest $(^{87}Sr/^{86}Sr)_{564}$ values are observed at the top of MCU I (0.70406) and MCU II (0.70498; Namur et al. 2010).

Anorthosite Blocks

Abundant anorthosite blocks cm- to tens of meters across are enclosed within cumulates of the Layered Series, and have been interpreted to be autoliths (Higgins 2005; Namur et al. 2011a) derived from the Upper Border Series. They are

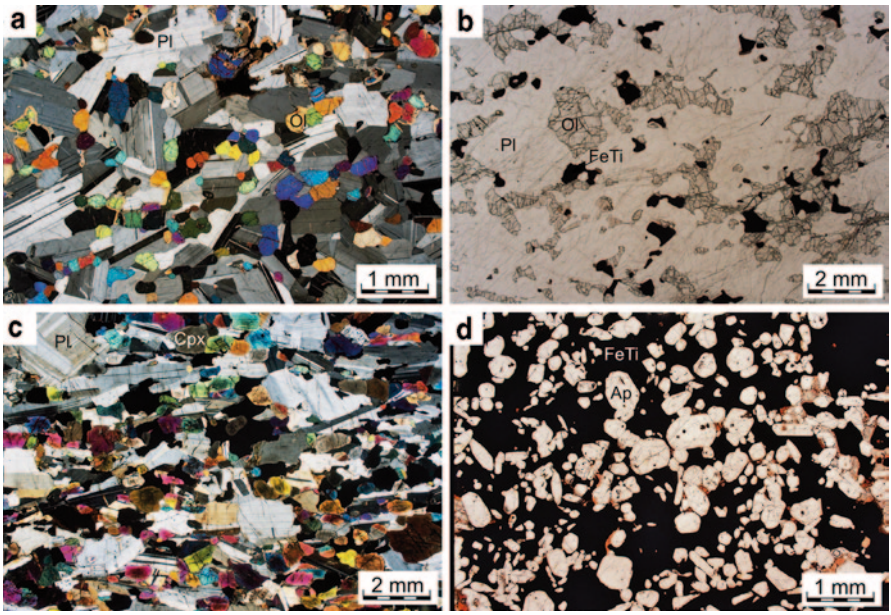

Fig. 11.6 Photomicrographs showing mineral textures and mineral assemblages in the Sept Iles Layered Series. **a** Troctolite (po-C) with randomly oriented, tabular plagioclase and millimeter-scale rounded olivine. DC9-2267.5; MCU I; cross-polarized transmitted light. This corresponds to the most primitive cumulus assemblage observed in the Sept Iles Layered Series. **b** Massive Fe–Ti oxide troctolite (pomi-C) containing large rounded grains of olivine, plagioclase and millimeter-scale anhedral patches of Fe–Ti oxides. DC 8-1309; MCU II; transmitted light. This photograph illustrates the appearance of large grains of cumulus Fe–Ti oxides (magnetite and ilmenite). **c** Gabbro (pmic-C) with long tabular plagioclase, prismatic clinopyroxene and millimeter-scale patches of Fe–Ti oxides. Sample ON05-35; MCU II; cross-polarized light. This photograph illustrates the appearance of cumulus clinopyroxene. Note the strong mineral lamination (especially for plagioclase and clinopyroxene), which is very common after the appearance of Fe–Ti oxides and clinopyroxene as cumulus phases. **d** Nelsonite sample from the apatite-bearing olivine gabbro unit (pomica-C) of MCU II. Note the presence of large crystallized melt inclusions (black spots) in apatite grains. Sample s9-218.8; MCU II; transmitted light. Other samples of apatite-bearing gabbro are more leucocratic than sample s9-218.8 and are dominated by plagioclase, olivine and clinopyroxene, with minor Fe–Ti oxides and apatite. *Pl* plagioclase; *Ol* olivine; *FeTi* Fe–Ti oxides; *Cpx* clinopyroxene; *Ap* apatite

mostly angular slabs and have sharp contacts with cumulates. Plagioclase ranges in colour from dark to light grey or white. Two types of autoliths are recognized: blocks of massive anorthosite (by far the most abundant) and blocks of laminated anorthosite. These blocks occur from the middle part of MCU I to the lower part of MCU III and are enveloped by gabbro (pomic-C; pmic-C; pomica-C) and Fe–Ti oxide troctolite (pomi-C). No autoliths have been observed in troctolite (po-C) in the lower part of MCU I and the upper part of MCU III (Fig. 11.5). Autoliths consist predominantly of plagioclase (84–96 vol.%), with minor olivine (0–6 vol.%), clinopyroxene (1–9 vol.%) and Fe–Ti oxides (0–4 vol.%). Low temperature alteration products are present in some of them.

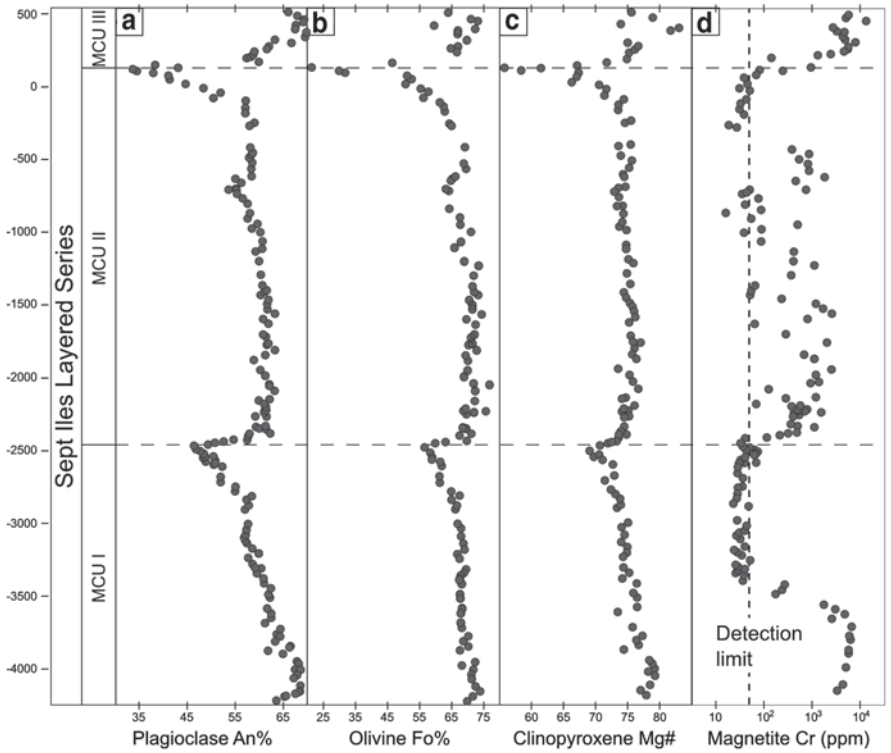

Fig. 11.7 Major- and trace-element variations in mineral compositions with stratigraphic position in the Layered Series. **a** Plagioclase (An%), **b** Olivine (Fo%), **c** Clinopyroxene (Mg#), **d** Magnetite Cr (ppm, log scale). *Dashed lines* represent boundaries between MCU. Note the evolution to lower An, Fo and cpx-Mg# in each MCU and the progressive reversals to more primitive compositions at the bottom of MCU II and MCU III. Also note the 60 m-thick marginal reversal at the base of MCU I. Data from Namur et al. (2010, 2012a). See Fig. 11.5. for details on where the samples were collected

Plagioclase shows a very restricted range of core compositions ($An_{60\text{-}68}$), with rims generally extending down to $An_{60\pm3}$. Olivine and clinopyroxene also show very restricted ranges of composition from Fo_{60} to Fo_{66} and cpx-$Mg\#_{68}$ to cpx-$Mg\#_{75}$, respectively. Sr-isotope ratios $(^{87}Sr/^{86}Sr)_{564}$ in plagioclase separates range from 0.70369 to 0.70386 and do not show any obvious trend when plotted against stratigraphic height in the Layered Series (Namur et al. 2011a).

The Upper Border Series

The Upper Border Series is composed of anorthosite, with minor leucotroctolite and leucogabbro (Higgins 1991). It is best exposed on the islands of the Sept Iles archipelago and the Marconi Peninsula. Two types of anorthosite with

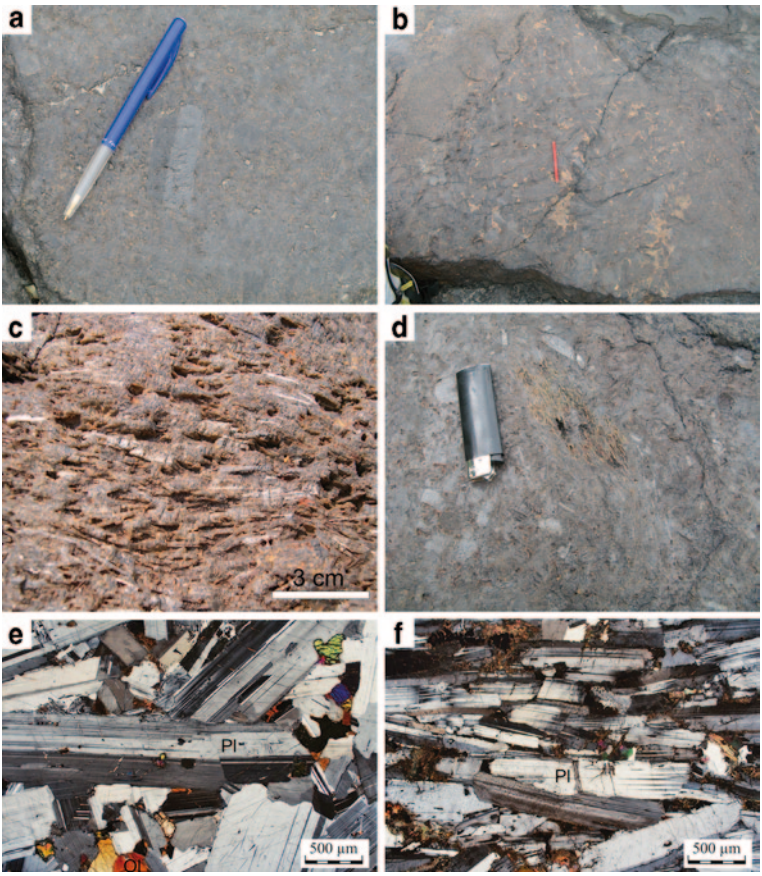

Fig. 11.8 Photographs (**a**–**d**) showing field relationships in the Upper Border Series and microphotographs (**e**–**f**) of representative samples of anorthosite. **a** Massive anorthosite of the Upper Border Series displaying a 5 cm-long plagioclase crystal set in a matrix of smaller plagioclase grains. **b** Massive anorthosite from the Upper Border Series showing interstitial syenitic to granitic material between plagioclase crystals. **c–d** Laminated anorthosite from the Upper Border Series. Altered clinopyroxene oikocrysts have been weathered out. **e** Massive anorthosite showing tabular, mm-scale, plagioclase grains and interstitial poikilitic olivine. M-07-55; cross-polarized transmitted light. **f** Strongly laminated anorthosite with large plagioclase grains, minor Fe–Ti oxide minerals and biotite in replacement of primary ferromagnesian minerals. GB-X1; cross-polarized transmitted light. *Pl* plagioclase; *Ol* olivine

very complex distribution are recognized (Higgins 1991): massive anorthosite (Figs 11.8a, b), which constitutes over 90 vol.% of the Upper Border Series, and laminated anorthosite (Figs 11.8c, d) which generally forms layers a few cm to tens of m-thick within the massive anorthosite. Where the layers can be traced, they generally terminate abruptly in the massive anorthosite within 1–20 m. The transition from massive to laminated anorthosite generally takes place over 1–5 cm. This lamination probably formed as a result of a simple shear due to

strong convection currents at the upper border of the magma chamber (Higgins 1991). Convection of the anorthositic mush may have also taken place and could explain how blocks of laminated anorthosite were transported to other parts of the magma chamber and enclosed within the massive anorthosite. Within the laminated anorthosite, the orientation of the lamination is generally not parallel to the overall structure of the intrusion and there are areas where the lamination diverges and wraps around pods of massive anorthosite up to 1 m long (Higgins 1991). In some areas, the laminated anorthosite is only present as angular to rounded xenoliths, 10 cm to 1 m long, enclosed in the massive anorthosite. Massive and laminated anorthosites both locally contain interstitial syenitic to granitic material (Fig. 11.8b), forming cm- to dm-scale pods, resulting from the percolation of silicic melt through the partly solidified anorthosite mush (Higgins 2005; Namur et al. 2011a, b).

Massive anorthosites are comprised of randomly oriented subhedral to euhedral plagioclase, with minor olivine, poikilitc clinopyroxene (up to 10 cm across), Fe–Ti oxides and very minor apatite, quartz, alkali-feldspar, amphibole, sulfides and minerals resulting from low-temperature hydrothermal alteration (Fig. 11.8e). Plagioclase generally forms 0.1–40 mm long grains, but some granophyric segregations contain plagioclase grains up to 1 m across. The large size of the crystals probably results from crystal size maturation in a crystal mush with an initial high liquid fraction (Higgins and Chandrasekharam 2007; Higgins 2011). These segregations are more common in the massive anorthosite than in the laminated anorthosite (Higgins 1991). Laminated anorthosites show a similar mineralogy but plagioclase grains display a very strong lamination (Fig. 11.8f).

Plagioclase, olivine and clinopyroxene show very restricted ranges of composition from An_{62} to An_{68}, Fo_{59} to Fo_{65} and cpx-$Mg\#_{66}$ to cpx-$Mg\#_{75}$, respectively. Bulk-rock compositions are high in SiO_2, Al_2O_3, CaO and Na_2O, reflecting the plagioclase-rich nature of these rocks (Table 11.3). $(^{87}Sr/^{86}Sr)_{564}$ in plagioclase separates range from 0.70356 to 0.70379 (Namur et al. 2011a).

The Upper Series

The Sept Iles Upper Series is comprised of syenite, granite and minor monzonite, cropping out on Marconi peninsula and the islands. There are several components that have complex field relationships and internal structures, some of which are revealed by the distribution of magmatic mafic enclaves (MME; Barbarin 2005). The two main components are: silicic rocks free of MME and MME-bearing silicic rocks (Higgins 2005; Hounsell 2006; Fig. 11.9a, b). Some MME contain plagioclase megacrysts and petrographically resemble the dolerite dykes in the Layered and Upper Border Series and Late Gabbro intrusions. The MME are generally ovoid, 1–10 cm long. MME locally occur as aggregates, forming m-scale mafic masses, or dyke swarms, separated by silicic rocks. There is a gradation from isolated blob-like MME to homogeneous mafic dykes through disjointed

Table 11.3 Bulk rock compositions of representative samples from the Upper Border Series. (Data from Namur et al. (2011a))

Sample	M-07-29	M-07-24	M-07-23	M-07-22	M-07-17	M-07-14	GB-05-04	GB-X1
Type	Massive	Massive	Massive	Massive	Massive	Massive	Massive	Laminated
SiO_2 (wt.%)	51.03	49.80	50.22	49.89	51.57	51.66	50.27	50.23
TiO_2	1.61	1.13	0.91	1.51	1.24	0.90	0.37	1.33
Al_2O_3	26.54	23.65	24.72	23.30	23.65	23.71	26.53	23.54
FeO_t	1.71	4.67	3.96	4.52	3.36	4.30	1.83	5.09
MnO	0.15	0.11	0.09	0.12	0.14	0.07	0.07	0.09
MgO	0.23	0.83	2.08	2.03	2.60	2.14	0.79	2.27
CaO	11.57	12.82	11.05	12.25	11.61	11.08	12.35	12.11
Na_2O	3.12	3.38	3.65	3.53	2.46	3.12	3.79	3.01
K_2O	0.59	0.51	0.93	0.82	1.01	1.26	0.24	0.57
P_2O_5	0.13	0.12	0.25	0.18	0.14	0.16	0.05	0.13
LOI	1.89	0.99	2.62	1.88	2.04	1.68	0.53	2.35
Total	98.57	98.01	100.48	100.03	99.82	100.08	96.82	100.72

dykes made up of MME aggregates. MME-free granite generally forms dm- to m-scale 'pillows' enclosed in MME-rich material (Fig. 11.9c). The MME-rich units occur between the pillows. In vertical section of the Upper Series, the amount of pillows drastically decreases from base to top (Fig. 11.9d). These field relationships suggest that the MME-rich magma formed first, but was not fully solidified when the MME-free granite was intruded (Higgins 2005).

Silicic rocks of the Upper Series are dominated by alkali-feldspar, plagioclase, quartz and amphibole, with minor clinopyroxene, Fe–Ti oxides, olivine, biotite, apatite, zircon, titanite, chlorite and fluorite (Higgins and Doig 1981; Hounsell 2006; Namur et al. 2011b). Alkali-feldspar ($Ab_{31}An_1Or_{68}$-$Ab_8An_0Or_{92}$) forms anhedral to subhedral tabular crystals with inclusions of plagioclase, quartz and amphibole. Plagioclase ($An_{25\text{-}18}$) forms small, antiperthitic, zoned, anhedral to tabular grains. Quartz forms 0.2–3 mm rounded grains, while edenitic amphibole ($Mg\#_{54\text{-}13}$) is represented by anhedral to subhedral dark-green to brown grains. Clinopyroxene (from Mg#51; $Ens_{25}Fs_{24}Wo_{51}$ to $Mg\#_{29}$; $Ens_{18}Fs_{34}Wo_{48}$) is only found as cores within amphibole grains. Minor subhedral to euhedral reddish biotite, frequently associated with fluorite, is observed in some samples. Fe–Ti oxides (magnetite: $Usp_{17\text{-}3}$; Ilmenite: $Hem_{1\text{-}0}$) occur as small (<2 mm) anhedral patches dominated by magnetite. Zircon and apatite locally form small euhedral grains.

Silicic rocks in the Upper Series have geochemical affinities with A-type granitoids (Loiselle and Wones 1979; Clemens et al. 1986; Eby 1990; Bonin 2007; Table 11.4) and are best described as ferroan alkalic to alkali-calcic granitoids (Frost et al. 2001; see below). They have high REE contents and display highly fractionated REE patterns with large negative Eu anomalies (Eu/Eu*: 0.22–0.86). Sr-isotope

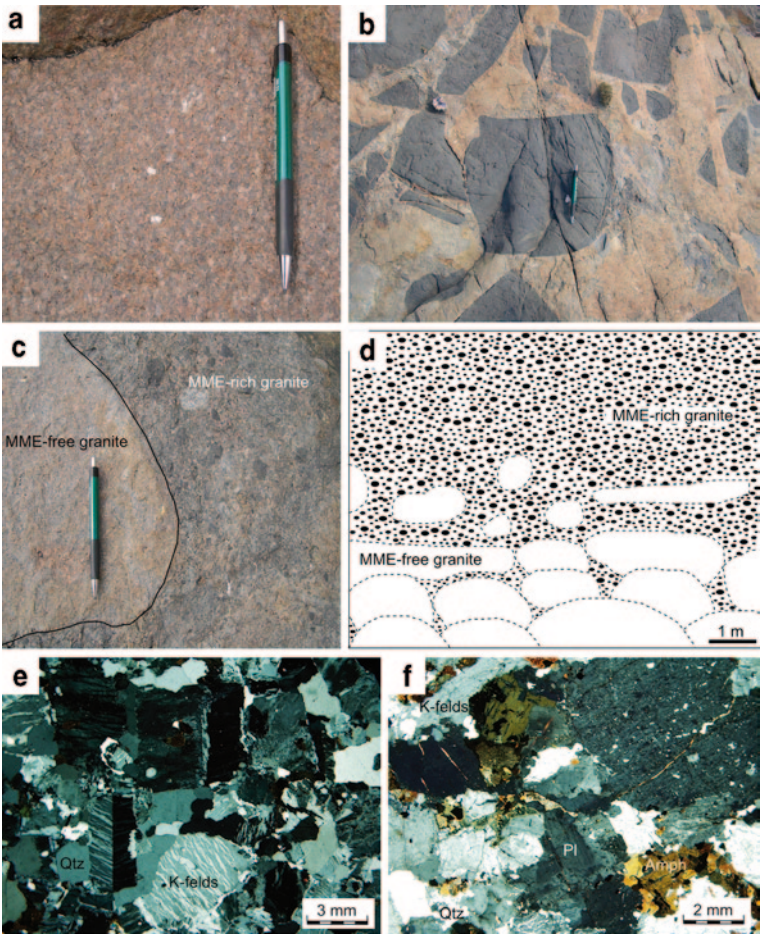

Fig. 11.9 Photographs (**a**–**c**) and sketch (**d**) showing field relationships in the Upper Series and microphotographs (**e**–**f**) of representative samples of granite. **a** Representative outcrop of *pink* magmatic mafic enclaves (*MME*)-free granite, Grande Basque Island. **b** Outcrop of *pink* granite containing abundant MME. The MME are mainly fine- to medium-grained dolerite similar to the dykes cutting the Upper Series, Marconi Peninsula. **c** Detail of the sharp contact between MME-rich granite facies and a 50 cm wide pillow of MME-free granite, Corossol Island. **d** Schematic relationships of MME-rich granite and MME-free granite as observed on Corossol Island (after Higgins 2005). Note that MME-free granite forms m-scale pillows surrounded by MME-rich material. MME-free granite pillows are abundant at the bottom of the section and their abundance decreases upwards. **e** Coarse-grained granite showing large alkali-feldspar and quartz grains. 03–05; cross-polarized transmitted light. **f** Coarse-grained granite with alkali-feldspar, plagioclase, quartz and amphibole grains. 03–42; cross-polarized transmitted light. *MME* magmatic mafic enclave; *K-felds* alkali-feldspar; *Pl* plagioclase; *Qtz* quartz; *Amph* amphibole

ratios have been measured in nine samples (from monzonite to granite) and were found to be slightly higher in MME-free rocks ($(^{87}Sr/^{86}Sr)_{564}$: 0.70412–0.70548) than in MME-bearing rocks ($(^{87}Sr/^{86}Sr)_{564}$: 0.70362–0.70369; Namur et al. 2011b).

Table 11.4 Bulk rock compositions of representative samples from the Upper Series and Pointe du Criard Sill. (Data from Namur et al. (2011b))

Sample	03-42	03-49	03-43	03-44	03-45	07-60	07-61
Unit	Monz.	Monz.	Syenite	Granite	Granite	Syenite	Granite
Type	US	US	US	US	US	PC	PC
SiO_2 (wt.%)	61.09	56.94	63.39	74.71	71.13	67.97	70.15
TiO_2	1.27	2.89	1.20	0.34	0.41	0.43	0.35
Al_2O_3	14.49	13.56	13.31	11.95	12.63	13.13	12.98
FeO_t	9.52	10.25	8.52	3.42	5.26	4.80	2.46
MnO	0.23	0.13	0.19	0.08	0.10	0.06	0.04
MgO	0.96	2.67	0.80	0.20	0.17	0.54	0.27
CaO	3.63	5.34	3.01	0.63	0.64	1.17	1.61
Na_2O	4.61	4.33	4.87	3.99	4.53	4.61	4.65
K_2O	3.40	2.24	3.69	4.68	4.32	4.87	4.92
P_2O_5	0.30	0.52	0.31	0.07	0.09	0.10	0.08
LOI	0.04	1.10	0.38	0.05	0.32	1.10	1.22
Total	99.51	99.94	99.64	100.09	99.57	98.75	98.70

US Upper Series, *PC* Pointe du Criard

Other Intrusive Components

Many dykes are found to crosscut the Layered Series and the Upper Border Series. They can be subdivided into two types: dolerite dykes and intermediate to silicic dykes. Dolerite dykes (0.1–1 m thick) are very fine-grained (0.1–0.5 mm) dominated by plagioclase, clinopyroxene and Fe–Ti oxides. They generally cut the layering at a high angle and dip steeply to the south. Intermediate and silicic dykes (and pods) are fine- to medium-grained (1–5 mm) and are generally found to cut apatite-bearing gabbros. They are dominated by subhedral, antiperthitic plagioclase, clinopyroxene, amphibole (primary grains or replacing clinopyroxene) and Fe–Ti oxides. Alkali-feldspar is a major phase in some samples. Minor quartz, biotite, apatite and zircon are observed in most samples. Dolerite and monzonite dykes in the Layered Series have bulk-rock compositions similar to the dolerite and monzonite in the Border Zone, with $(^{87}Sr/^{86}Sr)_{564}$ ratios ranging from 0.70353 to 0.70363.

The Pointe du Criard sill (Higgins 1990) is up to 50 m-thick and crops out over an area of 10 by 23 km, including all the islands and the Marconi peninsula. It was emplaced into the Upper Border Series and Upper Series of the Sept Iles layered intrusion. It is composed of three magmatic components: dolerite, leucogabbro and silicic rocks (Fig. 11.10a). The margins of the sill are made up of dolerite, which has fine-grained contacts with the host (anorthosite or granite). At the base of the sill, the dolerite unit is 0.1–6 m thick and locally contains plagioclase megacrysts that increase in proportion upwards. The dolerite grades into leucogabbro

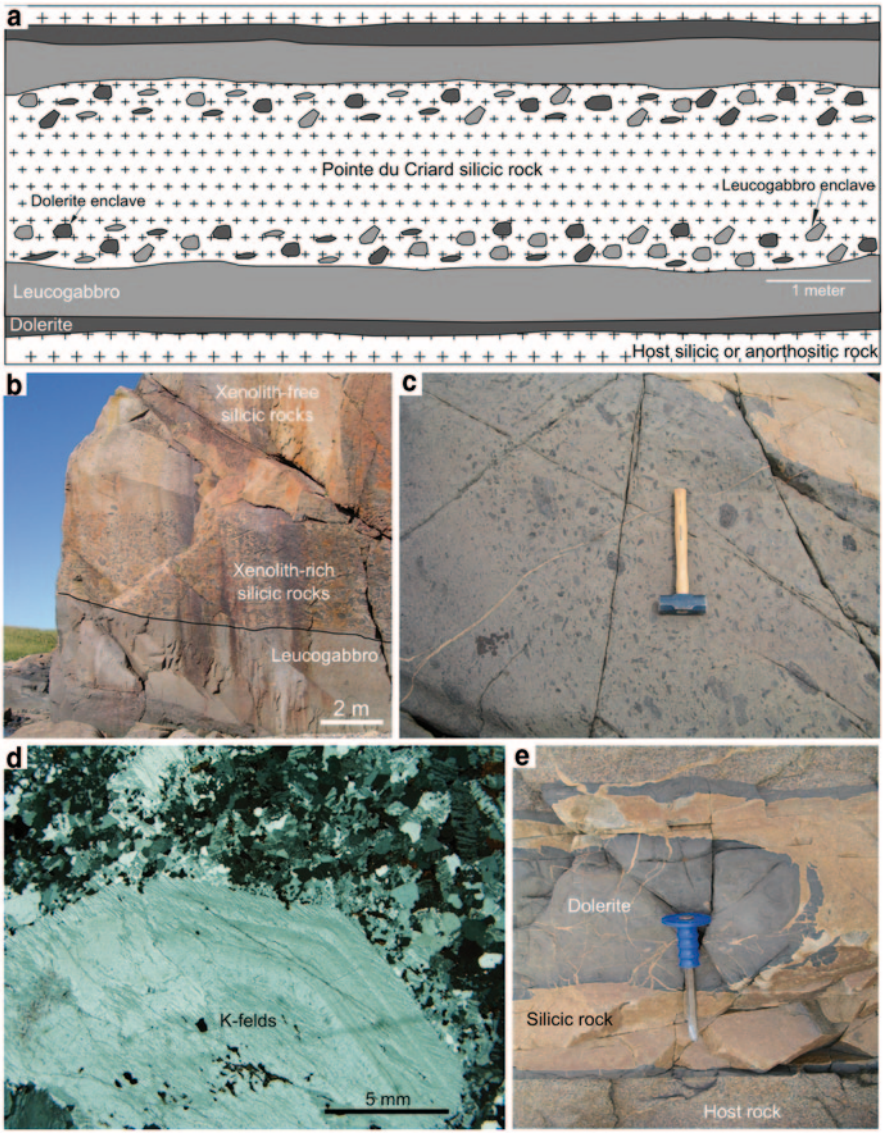

Fig. 11.10 **a** Schematic sketch of the Pointe du Criard sill displaying the succession of the three magmatic components: dolerite, leucogabbro and felsic rocks (after Higgins 2005). Enclaves of dolerite and leucogabbro are abundantly found in the lower and upper part of the felsic component. **b** Typical outcrop of the Pointe du Criard sill showing the succession of two different magmatic components: leucogabbro and silicic rocks. It should be noted that the external part of the silicic rocks contains abundant MME and mafic xenoliths. Size and abundance of MME and xenoliths decrease progressively toward the central part of the sill. The first dolerite component of the Pointe du Criard sill is not observed on this outcrop. **c** Close-up of the leucogabbro component of the Pointe du Criard sill. It is made up of fine-grained dolerite containing abundant centimeter-scale plagioclase phenocrysts. Plagioclase crystals larger than 20 cm have been observed in some outcrops. **d** Photomicrograph of porphyritic granite from the Pointe du Criard sill showing large alkali-feldspar grains in a fine-grained matrix comprised of alkali-feldspar, quartz, plagioclase and amphibole. Sample 03–08; cross-polarized transmitted light. **e** Representative composite dyke of dolerite-granite as observed in the Upper Series. Marconi Peninsula. *K-felds* alkali-feldspar

over a few cm to dm. The latter is 0.3–10 m thick and is mostly composed of large plagioclase crystals (Figs 11.10b, c). The silicic rocks constitute the bulk of the sill. At the base, leucogabbro grades into the silicic rocks over a few cm. The lower 1–3 m of the silicic rocks contains abundant enclaves of dolerite and leucogabbro. Some enclaves are highly elongated, up to 2 m long and only a few cm wide. The dolerite is dominated by plagioclase, clinopyroxene and Fe–Ti oxides, with minor olivine and orthopyroxene. The most plagioclase-rich parts of the leucogabbro unit are almost indistinguishable from the anorthosite of the Upper Series. The silicic rocks of the sill (Table 11.4) are readily distinguishable from those of the Upper Series, by a distinctive porphyritic texture and a low content of quartz. Large, zoned, and rounded crystals (up to 3 cm; Fig. 11.10d) of alkali-feldspar ($Ab_{15}An_0Or_{85}$-$Ab_9An_0Or_{91}$) float in a fine-grained, equigranular matrix (< 1 mm) dominated by perthitic alkali-feldspar, plagioclase (An_{1-5}), amphibole ($Mg\#_{18-22}$), Fe–Ti oxides (Usp_{3-14} and hem_1), ± quartz (Namur et al. 2011b). Relict cores of clinopyroxene ($Mg\#_{30-29}$) are locally observed in the central part of amphibole grains. Composite dolerite-granite dykes (Fig. 11.10e) may be part of the same event.

The Late Gabbro intrusions crop out on the southern part of Petite Basque Island and form the bulk of Grosse Boule Island (Higgins and Doig 1981). They consist of generally fine- to medium-grained gabbros, commonly with sub-horizontal layering. Angular blocks of anorthosite are locally present. They contain black plagioclase crystals up to a few centimeters long and resemble the anorthosite of the Upper Border Series. The petrography of these gabbros is little studied but they appear to be olivine gabbros. It is not clear if the abundant mafic dykes and locally composite dykes that cut the Upper Border Series and Upper Series are part of the same magmatic event.

Discussion

Composition and Origin of the Sept Iles Parental Magma

Petrography of dolerite samples from the Border Zone suggest that this unit might represent liquids chilled against cool country rocks during magma emplacement (Wager and Brown 1968; Hoover 1989; Namur et al. 2010). However, other examples of fine-grained rocks at the contact between country-rocks and coarse-grained gabbros have been interpreted as part of a marginal reversal made up of fine-grained cumulates (Egorova and Latypov 2012). In Sept Iles, the poor quality of outcrops and the absence of drill-cores in this unit makes impossible to evaluate the vertical and lateral mineralogical and geochemical evolution of this unit. However, Namur et al. (2010, 2011b) have shown that the most fine-grained dolerite samples (Fig. 11.3) have a ferrobasaltic composition (SiO_2: 45.9–52.4 wt.%; MgO: 6.29–3.61 wt.%; FeO_t: 13.2–17.1; Table 11.5) which is significantly different to

Table 11.5 Parent magma compositions of the Sept Iles Layered Series. (Data from Namur et al. (2010, 2011b)

Sample	05-45	07-01	07-48	07-180	Average
Location	Border zone	Dyke	Border zone	Border zone	
SiO_2 (wt.%)	48.56	48.51	48.65	48.53	48.56
TiO_2	2.91	2.88	2.78	2.82	2.85
Al_2O_3	14.62	14.13	14.59	14.67	14.50
FeO_t	15.10	14.82	15.06	14.50	14.87
MnO	0.29	0.23	0.21	0.21	0.24
MgO	5.53	5.56	5.14	5.65	5.47
CaO	9.97	9.61	9.47	9.79	9.71
Na_2O	2.90	2.76	2.81	2.63	2.78
K_2O	0.83	0.60	0.90	0.77	0.78
P_2O_5	0.36	0.72	0.36	0.82	0.57
LOI	0.00	0.23	0.23	0.03	–
Total	101.07	100.05	100.20	100.42	100.33
Rb (ppm)	8.97	16.2	18.1	8.03	12.8
Sr	472	531	517	523	511
Ba	458	509	421	515	476
Zr	90.8	126	264	126	152
Hf	2.81	3.52	–	–	3.17
Th	0.741	0.957	–	–	0.849
La	32.4	42.2	–	–	37.3
Ce	72.1	86.3	–	–	79.2
Pr	10.5	11.8	–	–	11.2
Nd	42.4	52.2	–	–	47.3
Sm	9.31	10.5	–	–	9.91
Eu	2.92	3.10	–	–	3.01
Gd	9.61	11.4	–	–	10.5
Tb	1.42	–	–	–	1.42
Dy	8.49	10.7	–	–	9.60
Ho	1.82	2.12	–	–	1.97
Er	4.96	6.00	–	–	5.48
Tm	0.699	–	–	–	0.699
Yb	5.58	5.59	–	–	5.59
Lu	0.581	0.876	–	–	0.729

the cumulates of the Layered Series. Moreover, most samples have slightly fractionated REE with a weak Eu anomaly (Eu/Eu*: 0.77–1.34) strongly suggesting that these samples have the composition of liquids having been chilled against the country rocks and that they do not represent cumulate rocks. Thermodynamic

calculations of phase equilibria with the MELTS (Ghiorso and Sack 1995) and other algorithms (Toplis 2005) have furthermore shown that the most primitive dolerite (highest Mg#; Table 11.5) is an adequate parent to the most primitive cumulates of the Layered Series (MCU I: An_{68}, Fo_{72}; MCU III: An_{72}, Fo_{71}). The Sept Iles parent magma is therefore inferred to be a ferrobasaltic liquid, relatively low in SiO_2 (ca. 48 wt.%), high in FeO_t (ca. 15 wt.%) and TiO_2 (3 wt.%), and moderately enriched in trace elements compared to primary melts of the primitive mantle. The concentrations of FeO_t and TiO_2 are significantly higher than in other ferrobasaltic layered intrusions such as Skaergaard (Hoover 1989; Toplis and Carroll 1995) and the Main and Upper Zones of the Bushveld Complex (Tegner et al. 2006) which, as shown below, has important implications for the Sept Iles sequence of crystallization. Typical primitive mantle-derived basaltic magmas have FeO_t contents between 7 and 10 wt.% and TiO_2 contents between 0 and 1 wt.% (Falloon et al. 1999; Danyushevsky et al. 2003); however, fractional crystallization of silicate phases can result in FeO_t and TiO_2 enrichment of residual liquids (Juster et al. 1989; Snyder et al. 1993; Toplis and Carroll 1995). The Sept Iles magma most probably represents an evolved basalt resulting from a previous process of fractionation of a more primitive magma in a deep-seated magma chamber. High FeO_t and TiO_2 basalts have also been observed in the Galapagos Spreading Centre and were interpreted by Juster et al. (1989) as resulting from 50 % fractionation of a typical mid-ocean ridge basalt (MORB) composition.

Crystallization of the Layered Series

Sequence of Crystallization

Detailed determination of mineral modes (see summary in Table 11.1) together with petrographical relationships in the Sept Iles Layered Series and detailed study of plagioclase-plagioclase-clinopyroxene dihedral angles indicate the following sequence of cumulus mineral appearance: plagioclase and olivine, followed by magnetite and ilmenite, then clinopyroxene and finally apatite (Fig. 11.5; Namur et al. 2010; Holness and Vernon 2015). Olivine disappears temporarily, probably as a result of high SiO_2 activity in residual melts (Morse 1990). The relative timing of Fe–Ti oxides, clinopyroxene and apatite appearance is supported by changes in the evolution of trace element concentrations in minerals and in bulk-rock compositions; (1) the evolution of Cr in magnetite changes from a trend of increasing content when Fe–Ti oxides are interstitial phases (low mode; po-C rocks) to a trend of decreasing content when they become liquidus phases (high mode; pomi-C rocks; Fig. 11.11a). We interpret this as the result of fractionation of olivine and plagioclase (po-C cumulates), in which Cr is incompatible, from the main magma body. As a consequence, the Cr content of the melt continuously increases, as does the melt trapped in the crystal mush. The interstitial magnetite crystallizes earlier and from a melt progressively enriched in Cr as we go upwards in stratigraphy,

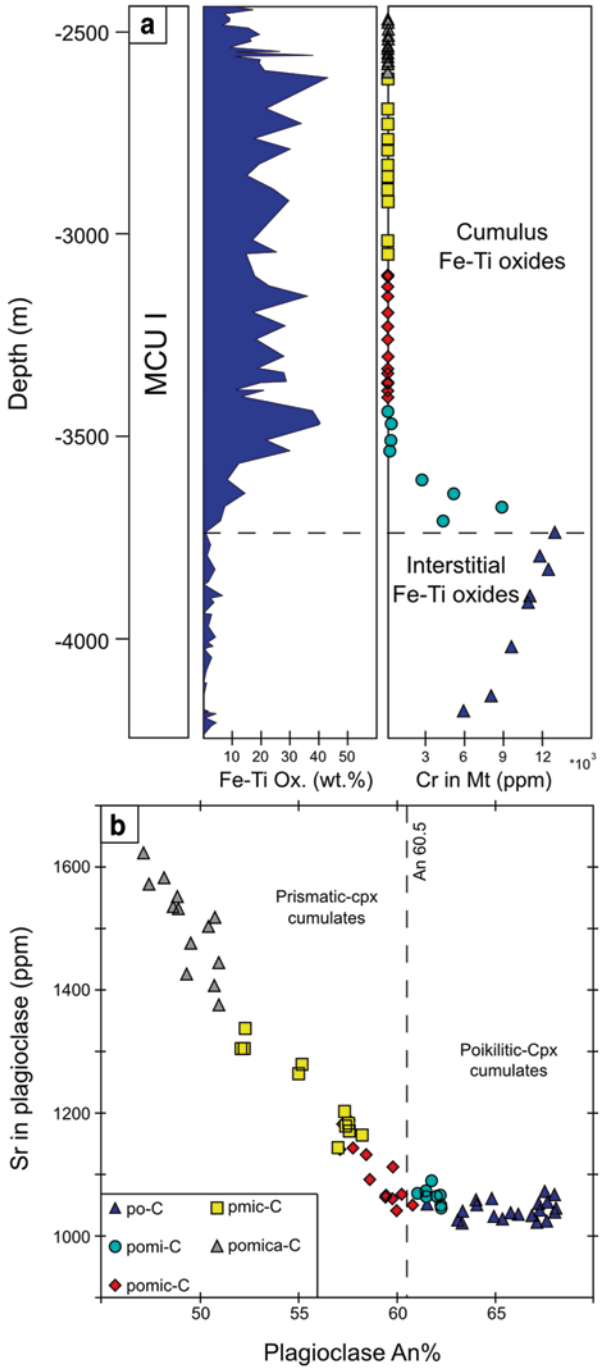

Fig. 11.11 **a** Stratigraphic variation of Fe–Ti (magnetite + ilmenite) oxide mode and Cr content in magnetite in MCU I. *Dashed line* represents the onset of cumulus Fe–Ti oxide crystallization which is marked by a change in the evolution of magnetite Cr-content. **b** Variation of An (%) vs Sr (ppm) in plagioclase separates from MCU I. Note the change in the slope at $An_{60.5}$, when clinopyroxene becomes prismatic and cumulus. *Ox* oxides; *Mt* magnetite; *Cpx* clinopyroxene

explaining the trend of increasing Cr in magnetite in po-C rocks. With the appearance of cumulus magnetite (and ilmenite; pomi-C rocks), Cr becomes highly compatible in the crystal matrix and the Cr-content of the liquid drops, explaining the upwards Cr-decrease observed in magnetite from the pomi-C unit; (2) the Sr-content in plagioclase starts to significantly increase at the appearance of cumulus clinopyroxene. This is because the saturation of this new phase changes the behaviour of Sr from a moderately compatible ($Kd^{Bulk} \sim 1$) element to an incompatible element ($Kd^{Bul} \sim 0.5$) in the cumulus matrix (Fig. 11.11b). The appearance of cumulus clinopyroxene is furthermore marked by a morphological change from poikilitic crystals to tabular crystals; (3) the saturation of apatite is recorded by a significant jump in the bulk-rock P_2O_5 content (Namur et al. 2010; Namur and Charlier 2012).

The most striking feature in the Sept Iles sequence of crystallization is the saturation of Fe–Ti oxides before clinopyroxene. This is in contrast with what is observed in many ferrobasaltic layered intrusions (McBirney 1989; Snyder et al. 1993; Wiebe and Snyder 1993) and other ferrobasaltic provinces (Carmichael 1964; Juster et al. 1989; Charreteur and Tegner 2013). Published experimental phase diagrams for ferrobasaltic liquids show that neither high water content nor high fO_2 can explain the sequence of crystallization observed in the Sept Iles Layered Series (Toplis and Carroll 1995; Botcharnikov et al. 2008). However, it has been shown that an increase in the FeO_t content of an anhydrous ferrobasalt from ca. 13 to ca. 16 wt.% results in the saturation of magnetite and ilmenite before clinopyroxene (Snyder et al. 1993; Toplis and Carroll 1995). It is therefore suggested that the early saturation of Fe–Ti oxides in Sept Iles is related to the high FeO_t content of the parent magma, and that differentiation took place with fO_2 close to the FMQ (Fayalite-Magnetite-Quartz) buffer.

Cryptic Layering and Filling of the Magma Chamber

The bottom of MCU I is characterized by the presence of a 60 m-thick marginal reversal of mineral compositions. By comparison with other intrusions, this may suggest that the initial filling of the magma chamber was gradual and involved a magma becoming increasingly primitive with time (Latypov et al. 2011). After the initial filling, fractional crystallization resulted in the stratigraphic succession of rocks with contrasting cumulus assemblages and an upward evolution towards lower An content of plagioclase, Fo content of olivine and Mg# clinopyroxene through MCU I and MCU II (Fig. 11.7). However, these trends are accompanied by gradual up-section increases in An%, Fo% and cpx-Mg# at the base of MCU II and MCU III. These changes in mineral compositions are accompanied by the disappearance of cumulus apatite and clinopyroxene. Cumulus Fe–Ti oxides also disappear at the base of MCU III. Large magma chamber replenishments are invoked to explain the cessation of magmatic differentiation in MCU I and MCU II as well as the observed shifts in mineral compositions and Sr isotopic ratios at the base of MCU II and MCU III. The retrograde change in mineral compositions

in reversals indicates that extensive mixing must have occurred during replenishment. Similar progressive magma chamber replenishments have been observed in the Fongen–Hyllingen layered intrusion (Wilson and Larsen 1982) and the Bushveld Complex (Roelofse and Ashwal 2012).

Extensive mixing between the resident and the injected liquid in MCU II and MCU III can occur when there is a low density, low-viscosity, contrast or if there is a high injection rate (Campbell and Turner 1986, 1989; Wiebe and Snyder 1993), which in turns mostly depends on the diameter of the feeder dyke (Wiebe and Snyder 1993). Extensive fractionation in each MCU of the Layered Series is expected to change significantly the density of residual liquids, especially after the saturation of Fe–Ti oxides (Wiebe and Snyder 1993). Slow magma injection should therefore lead to the formation of a zoned magma chamber and to an abrupt regression of mineral compositions, in contrast with what is observed at the base of MCU II and MCU III. Although the size of the magma feeder beneath Sept Iles is unknown, it is suggested that it must be large enough to allow magma injection at high rate and thorough mixing of magmas with contrasting densities, and presumably viscosities. This injection may have been as a vigorous fountain such that the proportion of the new to residual magma in the hybrid gradually increased (Campbell and Turner 1986, 1989). Strong convection in the magma chamber also further contributed to mixing between the injected and resident magma (Brandeis and Jaupart 1986).

The rate at which the liquids that formed MCU II and MCU III were injected into the magma chamber is unknown. A progressive, rather than stepwise, evolution of mineral compositions over 200–300 m suggests that the rate of injection is more or less identical to the rate of advance of the crystallization front (e.g. top of the crystal mush) at the bottom of the magma chamber. The volumes of injected magma at the base of MCU II and MCU III are also unknown but some constraints can be obtained about the relative volumes of injected vs resident magmas. The basal reversal within MCU III reaches mineral compositions with An%, Fo% and cpx Mg# similar to those observed at the base of MCU I. In contrast, minerals from the basal reversal of MCU II do not reach such primitive compositions. This dissimilarity indicates that the hybrid magma that crystallized MCU III was more primitive than that forming MCU II. The most evolved minerals from the Sept Iles layered series are observed at the top of MCU II, suggesting that MCU II has probably experienced a longer differentiation interval than MCU I before magma replenishment. It can thus be inferred that the proportion of residual liquid left at the top of MCU II was low. Consequently, when replenishment occurred at the base of MCU III, the low proportion of resident magma residual from MCU II was mixed with the primitive replenishing magma and the hybrid magma crystallized minerals with high An%, Fo% and cpx Mg#. In contrast, the replenishing magma at the base of MCU II was mixed with a higher proportion of resident magma residual from MCU I and the hybrid liquid thus crystallized less primitive minerals at the base of MCU II.

Minor Magma Chamber Replenishments

After the main magma chamber replenishment that initiated the formation of MCU II, plagioclase, olivine and clinopyroxene show relatively constant compositions over a cumulate sequence of 1.5 km (Fig. 11.7). In detail, these minerals show compositional cycles at a scale of ca. 200–500 m in which they first evolve towards slightly lower An-, Fo- and Mg# and then show minor reversals (1–4 An%; 1–3 Fo%; 1–3 Mg# %) to more primitive compositions (Fig. 11.12). Regressive sequences are also accompanied by temporary disappearances of cumulus clinopyroxene. In contrast to the silicate minerals, magnetite displays very large compositional variation within these cycles, with the Cr-content increasing from less than 10 ppm to more than 1000 ppm over the successive sequences.

Namur et al. (2010) have shown that neither pressure changes in the magma chamber (Panjasawatwong et al. 1995; Toplis 2005), nor changes in fO_2 (Toplis and Carroll 1995; Namur et al. 2012b) or crystallization from a stratified magma chamber (Tegner et al. 2006) can produce these reversals. In contrast, they suggested that these reversals in the lower part of MCU II resulted from minor replenishments by undifferentiated magma that mixed with the resident magma. These events were used to subdivide MCU II into seven cyclic units, 100–500 m thick, each corresponding to the differentiation products of a new batch of hybrid magma.

Large sequences of cumulate stratigraphy with relatively constant mineral compositions are observed in other layered intrusions and have been described in detail in the Bushveld Complex. They have recently been considered as a potential evidence that layered intrusions may not form by fractional crystallization of large volumes of magma but may instead result from the stacking of crystal mushes, with constant mineral compositions, injected from deep-seated magma chambers (Roelofse and Ashwal 2012; see also details in Cawthorn 2012). Here, we show that this interpretation is largely biased by the use of silicate mineral compositions only; minerals that are not sensitive enough to record small-scale magma chamber replenishments by primitive magma. However, when other minerals such as magnetite are considered it is apparent that these large intervals of stratigraphy reflect cycles with progressive differentiation interrupted by many injections of primitive magma.

Expansion of the Magma Chamber

During the initial filling of the magma chamber that crystallized MCU I, the chamber expanded laterally until it reached an unknown initial diameter. After this initial filling, the two large magma chamber filling events that respectively formed MCU II and MCU III, as well as minor replenishments within MCU II, contributed to significantly enlarge the size of the Sept Iles magma chamber. Given the relative thickness each of MCU, the magma column was however never thicker than 2.5 km. The initial magma chamber was presumably in the

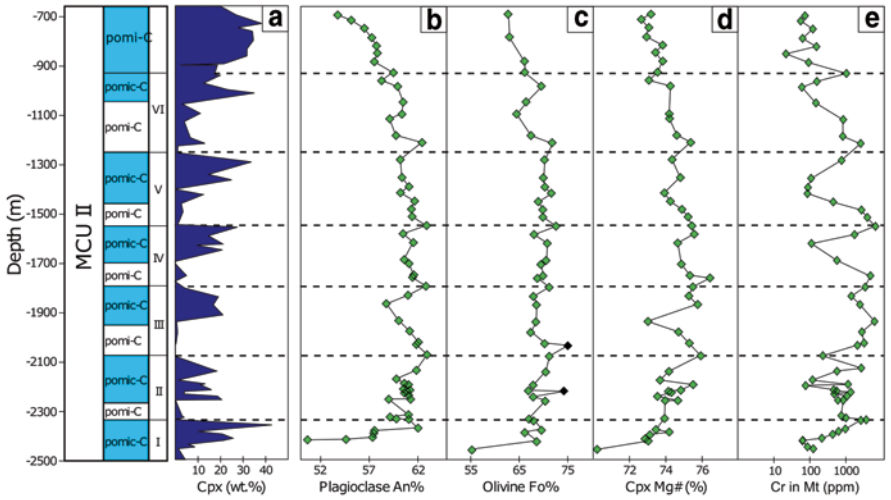

Fig. 11.12 Modal and compositional stratigraphic variations in the lower part of MCU II (from −2500 to −700 m). **a** Mineral mode of clinopyroxene; **b** An content of plagioclase; **c** Fo content of olivine; **d** Mg-number of clinopyroxene; **e** Cr content of magnetite. I–VII represent the seven cyclic units of MCU II. *Dashed lines* represent the boundaries between cyclic units. The two *black diamonds* in the olivine trend are samples that are interpreted to have undergone intense subsolidus re-equilibration (see Namur et al. 2010). Note that at the bottom of each cycle minerals evolve to more evolved compositions (lower An, Fo, cpx-Mg-number, low magnetite Cr-content) while at the top of the cycles they evolve to more primitive compositions. The relatively low mode of clinopyroxene at the bottom of each cycle should also be noted

form of a sill that progressively deformed to a dinner plate shape by subsidence of the floor due to the weight of cumulate rocks, a process that occurred contemporaneously with crystallization (Higgins 2005). It probably started during the crystallization of MCU I and continued during crystallization of MCU II and MCU III. It is therefore likely that the liquids having formed MCU II and MCU III were injected into a dinner-plate shaped magma chamber, which may cause some angular inconformity in the layering (modal and/or cryptic) at the interface between rocks from two successive MCUs (Wilson and Larsen 1982). Similarly to other major layered intrusions such as Bjerkreim–Sokndal (Wilson et al. 1996) and the Bushveld Complex (Kruger 2005), it is likely that the magma chamber did not only expand vertically but also laterally during magma injections that formed MCU II and MCU III. The fact that MCU II is found to be in contact with the Border Zone in the north-eastern part of the Sept Iles layered intrusion may confirm this idea. This probably indicates that the Border Zone was formed incrementally by a series of magma injections that formed the major MCUs and that the magma chamber increases laterally after each of these injections. Unfortunately, the poor quality of outcrops on the Sept Iles mainland makes the relationship between the cumulate rocks of the Layered Series and the Border Zone poorly constrained.

The Sept Iles Liquid Line of Descent and the Origin of Ferroan Granites

Liquid Compositions and Formation of the Silicic Melts

A series of rocks from the Sept Iles Intrusive Suite have petrographic characteristics suggesting that they might represent liquid compositions. The most important of them are (1) rocks from the Sept Iles Border Zone (chilled margin; see representative samples in Table 11.5), (2) dykes cross cutting the Layered Series (Table 11.5) and (3) silicic rocks from the Upper Series and Pointe du Criard sill (Table 11.4). The major and trace element bulk-rock compositions of these samples as well as $(^{87}Sr/^{86}Sr)_{564}$ ratios have been presented in Higgins and Doig (1986) and Namur et al. (2011b).

Dolerite samples from the Border Zone, dykes cutting the Layered Series and silicic rocks from the Upper Series and the Pointe du Criard define a coherent compositional trend from basalt to rhyolite, with a small amount of intermediate trachyandesite and trachyte compositions (see below), straddling the boundary between subalkaline and alkaline fields in a TAS diagram (Fig. 11.13a). All the samples are located within the tholeiitic field of the AFM diagram (Fig. 11.13b), while the most evolved compositions fall within the field of ferroan alkalic to alkali-calcic granitoids (Fig. 11.13c, d; Frost et al. 2001). Major elements from basalt to rhyolite display coherent trends when plotted as a function of a differentiation index such as SiO_2, with some elements continuously decreasing (e.g. CaO, MgO), continuously increasing (K_2O) or first increasing and then decreasing (FeO_t, TiO_2, Na_2O, P_2O_5). REE contents continuously increase from basalt to rhyolite, while a progressively deeper negative Eu anomaly develops. Other incompatible elements (e.g. Ba, Rb) increase from basalt to rhyolite, while elements such as P, Ti and Sr are progressively depleted, forming large negative anomalies in N-MORB normalized trace element diagrams.

Continuous major and trace element trends from basalt to rhyolite suggest that the fractionation of cumulus phases observed in the Layered Series from the Sept Iles parent magma might be responsible for the genesis of intermediate and silicic liquids in the Sept Iles layered intrusion. This was first modelled using mass-balance equations by Higgins and Doig (1986) and then in more detail by stepwise least-squares mass regressions by Namur et al. (2011b). Modelling indicates that the maximum enrichment in FeO_t (17 wt.%; saturation of Fe–Ti oxides) is reached when the liquid SiO_2 content is 47 wt.% and the proportion of residual liquid (F) is 0.86 (Fig. 11.14). The appearance of cumulus Fe–Ti oxides (Fig. 11.14) is responsible for a progressive SiO_2 enrichment of residual liquids. Clinopyroxene and apatite saturations are reached when $F = 0.72$ and 0.52, respectively. Further fractionation of ferrogabbros drives residual liquids towards further SiO_2 enrichment, with monzonitic and granitic compositions being produced when F is 0.32 and 0.08, respectively. Fractional crystallization has also been tested using trace elements,

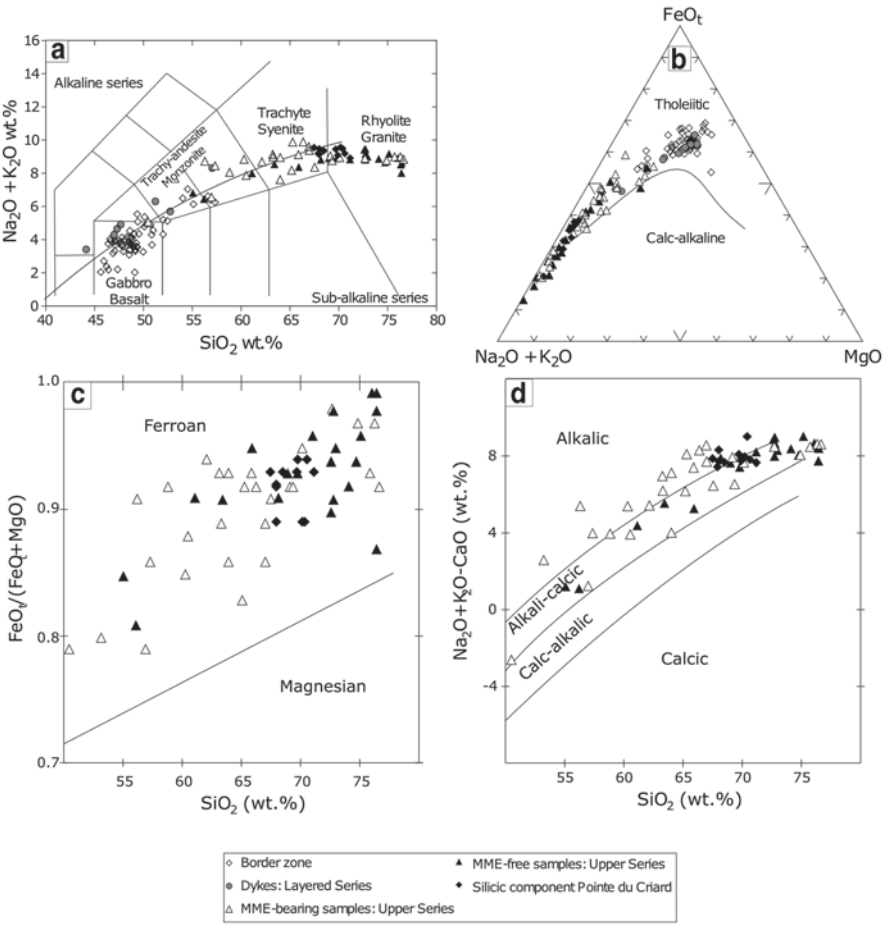

Fig. 11.13 The compositions of fine-grained dolerite samples (*Border Zone*), dykes (*Layered Series*) and silicic rocks (*Upper Series*) from the Sept Iles Intrusive Suite plotted in: **a** The total alkali-silica (*TAS*) diagram (Na_2O+K_2O) vs SiO_2. The limit between the alkaline and sub-alkaline series is shown by the *curved line* (Irvine and Baragar 1971). Observe that the whole set of samples forms a single consistent trend from basaltic to rhyolitic compositions at the boundary between the alkaline and sub-alkaline series. **b** The AFM diagram showing the limit between tholeiitic and calc-alkaline fields (Irvine and Baragar 1971). Sept Iles samples fall within the tholeiitic compositional field. **c** Major element geochemical classification of silicic samples in the $FeO_t/(FeO_t+MgO)$ vs SiO_2 diagram (Frost et al. 2001). **d** Major element geochemical classification of silicic samples in the Na_2O+K_2O–CaO vs SiO_2 diagram (Frost et al. 2001)

with the Rayleigh equation, appropriate partition coefficients (see Namur et al. 2011b), together with mineral and liquid proportions obtained by mass-balance calculations for major elements. The trace element patterns of monzonitic, syenitic and granitic melts are well reproduced by fractional crystallization of the parent magma for F = 0.3, 0.2 and 0.1, respectively (Fig. 11.15).

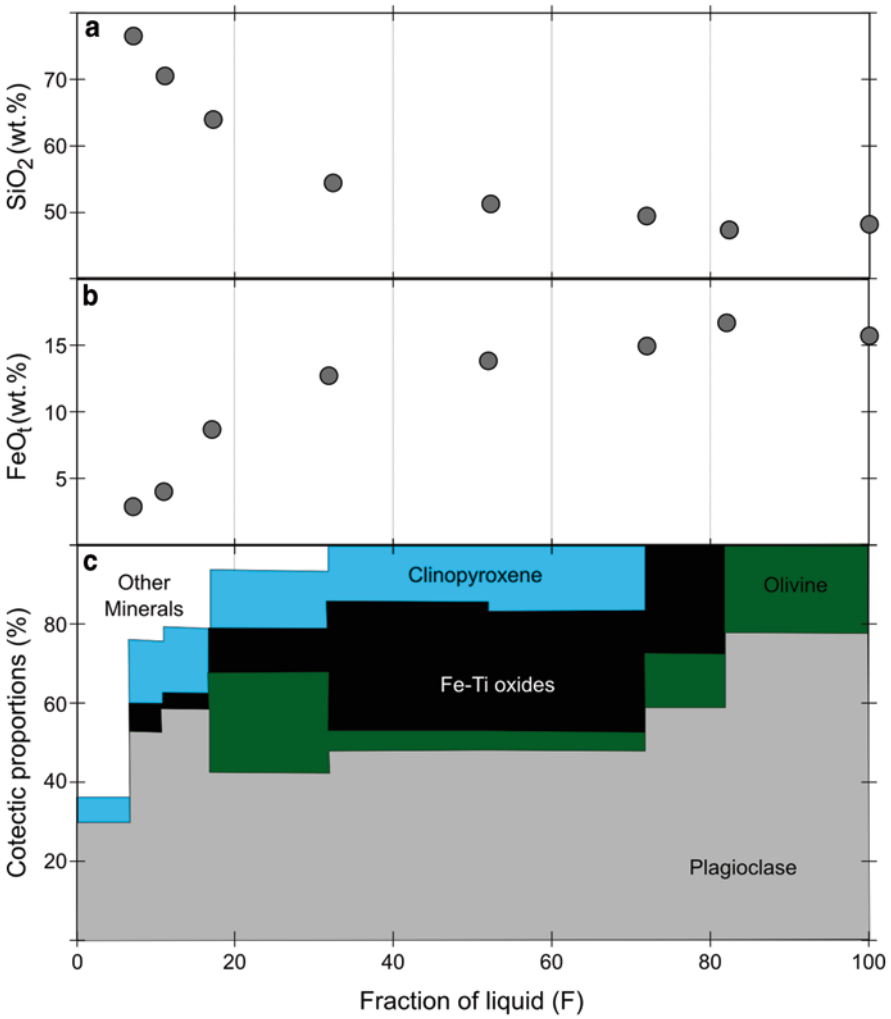

Fig. 11.14 Results of mass-balance calculations showing the best fit results for the Sept Iles liquid line of descent. **a** SiO_2 in residual melts vs F (fraction of remaining melt). **b** FeO_t vs F. **c** Calculated mineral cotectic proportions for each cumulus assemblages. Mineral cotectic proportions are relatively similar to mineral modes presented in Namur et al. (2010) and determined by point counting on polished thin sections. Other minerals = amphibole, biotite, alkali-feldspar and apatite. *Solid circles* in (**a**) and (**b**) represent the liquid compositions used in the calculations by Namur et al. (2011b). Calculations have been performed for successive liquids (*circles*; decreasing F) by removing minerals in the proportions shown in (**c**). The starting parental magma composition is presented in Table 11.5. Calculated mineral compositions can be found in Namur et al. (2011b). Note that the FeO content of residual melts decreases after the saturation of *Fe–Ti oxides*, a much discussed issue for the Skaergaard intrusion

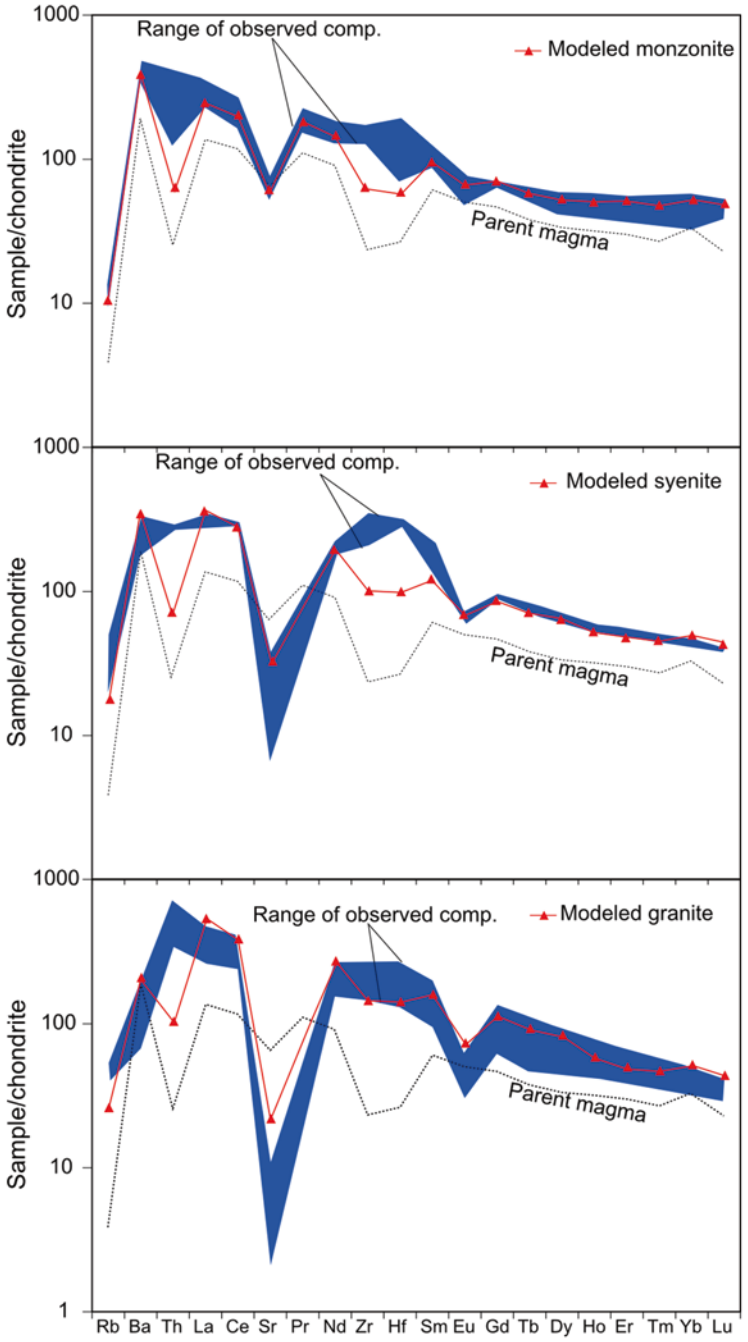

Fig. 11.15 Chondrite-normalized trace element variation diagrams showing the compositions of residual melts produced by fractional crystallization (Rayleigh fractionation) and comparison with the compositions of rocks (*blue fields*) observed in the Sept Iles layered intrusion. **a** monzonitic, **b** syenitic and **c** granitic liquids. Mineral proportions used in calculations are from major-element mass-balance calculations (see Fig. 11.14). Partition coefficients used in calculations can be found in Namur et al. (2011b)

Comparison of fractional crystallization models with the composition of Sept Iles rocks therefore suggests that protracted fractional crystallization is a realistic way to produce the silicic liquids observed in Sept Iles. Other processes such as partial melting of gneissic country rocks (Lightfoot et al. 1987; Patino Douce 1997) or a mafic source in the lower or upper crust (Beard and Lofgren 1991) can also produce A-type granites. However, theoretical models performed by Namur et al. (2011b) have shown that melting of none of these sources can produce melts with compositions similar to those of the granites observed in Sept Iles. It is therefore suggested that the continuous trend from basalt to rhyolite (Fig. 11.13) represents the actual Sept Iles liquid line of descent. This is also in agreement with field relationships convincingly showing that no trace of silicic melt is present in cumulate rocks more primitive than apatite-bearing gabbros. This unambiguously suggests that silicic magmas are residual after extensive fractionation of troctolites and gabbros in the Layered Series. In contrast to the Skaergaard intrusion for which the liquid line of descent is highly debated (Hunter and Sparks 1987; McBirney and Naslund 1990; Toplis and Carroll 1996; Tegner 1997; Thy et al. 2009), the Sept Iles layered intrusion therefore shows an undisputable evidence of liquid line of descent evolving towards SiO_2-enrichment after Fe–Ti oxide saturation. This trend is moreover in perfect agreement with liquid compositions observed in volcanic ferrobasaltic provinces worldwide (Charlier et al. 2013).

Role of Country Rock Contamination

There is a remarkable covariation of the composition of cumulus minerals and their Sr isotopic ratios within each MCU in the Layered Series (Fig. 11.16a). This suggests that assimilation of country rocks was taking place continuously during the solidification history of Sept Iles (Tegner et al. 2005), and that this process, together with fractional crystallization, contributed to the geochemical composition of the cumulates and the residual liquids. Contamination probably resulted from the incorporation of blocks of country rocks into the magma before emplacement or possibly in the chamber itself. A contributing factor may have been strong tectonic activity, as major St Lawrence Rift system faults cut the intrusion. It is therefore of interest to determine whether or not country-rock assimilation contributed to the SiO_2 enrichment of the residual melts. The Sr content of the Sept Iles parent magma is estimated to be 511 ppm, while its initial Sr-isotopic composition was 0.70353 (Namur et al. 2010, 2011b). Three main types of country rocks occur in the Grenville province around Sept Iles: (1) metagabbro (Sr: 260 ppm, $(^{87}Sr/^{86}Sr)_{564}$: 0.7094); (2) gneissic monzonite (Sr: 230 ppm, $(^{87}Sr/^{86}Sr)_{564}$: 0.7189); (3) cordierite-bearing leucocratic gneiss (Sr: 97 ppm, $(^{87}Sr/^{86}Sr)_{564}$: 0.7746). The amount of country rock assimilated during the solidification of the Sept Iles layered intrusion was modelled using the assimilation-fractional crystallization (AFC) equations of DePaolo (1981) and the Sr

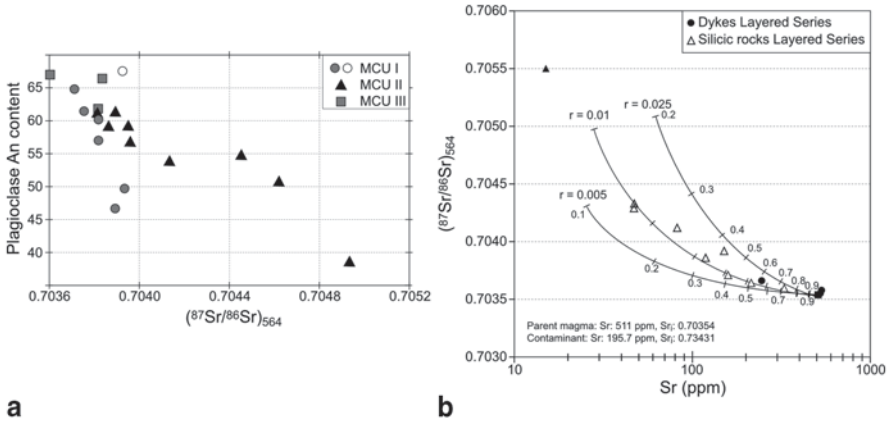

Fig. 11.16 Sr isotopic data in the Sept Iles layered intrusion. **a** Binary diagram showing the An-content and $(^{87}Sr/^{86}Sr)_{564}$ ratio of plagioclase separates from the Layered Series. Note how the Sr isotopic ratios are anticorrelated with the An-content of plagioclase, which is considered as an index of differentiation of the Sept Iles magma. This indicates that contamination from country-rock material was taking place during the solidification of the Sept Iles Layered Series. **b** $(^{87}Sr/^{86}Sr)_{564}$ vs Sr for Sept Iles liquids. The *curves* show AFC models calculated following DePaolo (1981) for various mass ratios (0.005–0.025) of assimilated to fractionated material. Numbers along AFC lines give the fractions of residual liquids. Sr and isotopic data for the Sept Iles parent magma and the contaminant are shown for reference. This diagram indicates that the evolution of Sr-isotopic ratios in the Sept Iles layered intrusion can be modelled with a very low amount of contamination from the country-rock material (e.g. 2.5%; see text for details). Data from Namur et al. (2010, 2011b).

isotopic compositions of Sept Iles liquids (Namur et al. 2011b; Fig. 11.16b). The average composition of the three distinct types of country rocks was used as the contaminant component (Sr: 196 ppm, $(^{87}Sr/^{86}Sr)_{564}$: 0.7343). D_{Sr}^{Bulk} was set to 1.6 for the F range from 1.0 to 0.7, and to 2.1 for further differentiation. Results of AFC modelling indicate that the Sr isotopic composition of Sept Iles rocks can be reproduced with only very minor crustal assimilation. A ratio (r) between 0.01 and 0.025 of assimilated to crystallized material is sufficient to match adequately the observed Sr isotopic compositions of Sept Iles liquids (Fig. 11.16b). The amount of assimilation is even lower than 1% when using the most radiogenic country rocks (cordierite-bearing gneiss) as the main contaminant. It is however slightly higher (5%) when using the least-radiogenic country rocks (metagabbro). AFC models therefore suggest that country-rock assimilation played a very minor role in the geochemical evolution of Sept Iles melts.

Paucity of Intermediate Liquid Components

Most of intermediate compositions along the Sept Iles liquid line of descent contain abundant mafic enclaves (MME, Fig. 11.13). They therefore represent hybrid

magma with intermediate bulk compositions, and create an artificial continuous differentiation trend between the most evolved basalts at 57 wt.% SiO_2 and the most primitive MME-free granitoids at 67 wt.% SiO_2. The very low proportion of true intermediate compositions observed along the Sept Iles liquid line of descent, generally referred to as a 'Daly gap' has been observed in other magmatic systems and has traditionally been interpreted as resulting from magma passing through all the intermediate compositions (intermediate liquid SiO_2 contents) for only a small drop of temperature, so only a small proportion of intermediate liquid is actually produced (Grove and Donnelly–Nolan 1986; Toplis and Carroll 1996; Peccerillo et al. 2003; Tegner et al. 2006). However, this model is inconsistent with mass-balance calculations showing that 15 % of fractionation is required to cover the whole range of intermediate compositions and that only a further 10 % of fractionation is required to drive residual liquids across the compositional range of highly silicic melts (67–77 wt.% SiO_2). Silicic rocks are more abundant than intermediate rocks in the Sept Iles layered intrusion (Fig. 11.13), suggesting that the low proportion of intermediate melts represented at Sept Iles cannot be related to a low volume of intermediate melt produced by fractional crystallization.

Minerals in apatite-bearing gabbros from the Layered Series MCU II, especially apatite, contain abundant, 10–120 μm, polycrystalline crystallized melt inclusions of two types: a granitic Si-rich composition and a Fe-rich ferrobasaltic composition. Single inclusions locally show evidence for unmixing between the two compositions, and Si-rich and Fe-rich compositions are therefore interpreted as immiscible melts (Charlier et al. 2011). Silicate liquid immiscibility in the Sept Iles magma is interpreted as being responsible for the paucity of intermediate liquid compositions along the liquid line of descent. Immiscibility started by the intersection of Sept Iles residual liquids with a subliquidus binodal (Fig. 11.17a). This process started when the residual liquid reached a monzonitic composition (57 wt.% SiO_2; 10 wt.% FeO_t), e.g. the start of the Daly gap, producing highly contrasting immiscible melts and no melt of intermediate composition (as opposed to fractional crystallization; Fig. 11.17a). Upon cooling, both immiscible melts kept solidifying and crystallized cumulate rocks with identical mineral compositions (but contrasted mineral modes), while the residual liquids evolved along the bimodal. During this process, the bulk liquid composition (i.e. the sum of the two immiscible melts) was continuously enriched in SiO_2 and depleted in FeO_t (Fig. 11.13). Ultimately, the bulk liquid compositions left the two liquid field (Fig. 11.17a), producing a single homogeneous liquid that further evolved to produce the residual granites of the Upper Series, which are satisfactorily modelled by a simple fractional crystallization process (Fig. 11.14). Immiscibility in Sept Iles was therefore a furtive event, with no influence on the composition of liquids along the liquid line of descent, except that this process was responsible for the absence of primary intermediate melts (Fig. 11.17b).

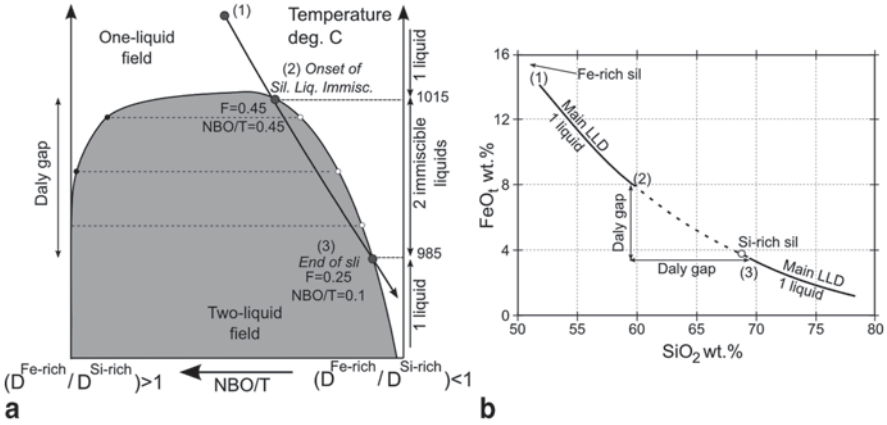

Fig. 11.17 Schematic illustration of the evolution of the Sept Iles liquid line of descent through a two-liquid field. The morphology of the binodal is based on Charlier and Grove (2012). The Sept Iles liquid reaches the binodal on the Si-rich side at ca. 1015 °C when F = 0.45 (Namur et al. 2012a) and splits into two conjugate immiscible melts (Fe-rich and Si-rich). Immiscible melts produce cumulate rocks (ferrogabbros) with identical minerals but in contrasting proportions. Fractional crystallization of ferrogabbros drives the bulk-liquid composition (sum of Si-rich and Fe-rich immiscible melts) towards further SiO_2-enrichment (see Fig. 11.14) and the bulk-liquid composition ultimately leaves the two-liquid field at ca. 985 °C (F = 0.25). This results in the formation of a single stable liquid after the episode of silicate liquid immiscibility. Further differentiation of a single liquid produces the granites from the Sept Iles Upper Series (see text for details and models in Fig. 11.14). *sli* silicate liquid immiscibility; $D^{Fe\text{-}rich}$ elements partitioning into the Fe-rich immiscible melt; $D^{Si\text{-}rich}$ elements partitioning into the Si-rich immiscible melt. **b** FeO_t vs SiO_2 diagram showing the result of the silicate liquid immiscibility episode on the Sept Iles liquid line of descent. The only evidence for the immiscibility episode is the absence of intermediate liquid compositions (Daly gap; Charlier et al. 2013). *sil* silicate immiscible melt

Implications of the Liquid Line of Descent for Magma Chamber Processes

Plagioclase Flotation in Ferrobasalts

Plagioclase in anorthosite from the Upper Border Series shows a very restricted range of composition ($An_{62\text{-}68}$), which is moreover similar to the plagioclase composition in anorthosite blocks (autoliths) in the Layered Series. It is also identical in composition to the plagioclase found in troctolites (po-c) and Fe–Ti oxide troctolites (pomi-C) in the Layered Series, but is significantly more primitive than the plagioclase from the gabbros (pomic-C, pmic-C and pomica-C; $An_{31\text{-}60}$; Fig. 11.7). A similar relationship is observed for trace elements and Sr-isotope ratios in plagioclase (Namur et al. 2011a). A genetic link between plagioclase in the Upper Border Series, in autoliths and in troctolites from the Layered Series seems therefore evident.

The origin of anorthosite in the Sept Iles layered intrusion has been investigated by Namur et al. (2011a) using density calculations for liquids and plagioclase (Bottinga and Weill 1970; Niu and Batiza 1991), oxygen fugacity along the FMQ buffer and a pressure of 3 kbar. Liquids used for density calculations correspond to the samples plotted in Fig. 11.13. A water content of 0.4 wt.% H_2O has been assumed for the parent magma. For each liquid sample, the composition of equilibrium plagioclase has been calculated using the equations of Namur et al. (2012b).

The calculated density of the Sept Iles parent magma is 2.70 g/cm^3, increasing due to fractionation of troctolites to 2.75 g/cm^3 at saturation in Fe–Ti oxides, and then decreasing to 2.16 g/cm^3 in granitic melts as the result of Fe–Ti oxide troctolite and gabbro fractionation (Fig. 11.18a). Calculated plagioclase compositions range from An_{68} to An_{34}, in perfect agreement with plagioclase compositions in the Layered Series, and plagioclase density decreases from 2.69 to 2.64 g/cm^3 with differentiation.

Density calculations indicate that plagioclase was buoyant in primitive melts, but that plagioclase became denser than the equilibrium melt soon after the saturation of Fe–Ti oxides, when the liquid reached 49 wt.% SiO_2. Primitive liquids in which plagioclase was buoyant were in equilibrium with a very restricted range of plagioclase composition ($An_{61\text{-}69}$), identical to that observed in Sept Iles anorthosite (Fig. 11.18a). In contrast, more evolved plagioclases ($An_{<60}$), were in equilibrium with evolved liquids (>49 wt.% SiO_2) and were no longer buoyant. Formation of the anorthosite therefore resulted from the flotation of primitive plagioclase ($An_{>60}$) and its accumulation at the roof of the magma chamber (Fig. 11.18b). The decrease of liquid density subsequent to the saturation of Fe–Ti oxides inhibited further flotation of plagioclase (Fig. 11.18b). Furthermore, the anorthosite from the Upper Border Series became denser than the main magma body. As a consequence, anorthositic blocks sank into the magma chamber, forming the autoliths blocks observed in the Layered Series.

As illustrated above, plagioclase ($An_{>60}$) that was buoyant is present in the Layered Series troctolites and the most primitive Fe–Ti oxide troctolites. This indicates that not all of the plagioclase grains floated and accumulated at the roof of the magma chamber. We interpret this as a consequence of *in situ* crystallization. This mechanism prevents flotation due to attachment of the crystals to the floor of the magma chamber. Formation of coherent three-dimensional chains of crystals (Philpotts and Carroll 1996; Philpotts et al. 1998) may also have contributed to the retention of plagioclase grains on the chamber floor. Comparison between the proportion of plagioclase in the troctolites of the Layered Series (67.5 % on average; Namur et al. 2010) and estimated plagioclase cotectic proportion in equilibrium melts (78 %; Namur et al. 2011b) can be used to put some constraints on the efficiency of *in situ* crystallization. These values confirm that plagioclase is missing in the Layered Series, and that more than 10 % of the liquidus plagioclase accumulated at the top of the magma chamber to form the Upper Border Series.

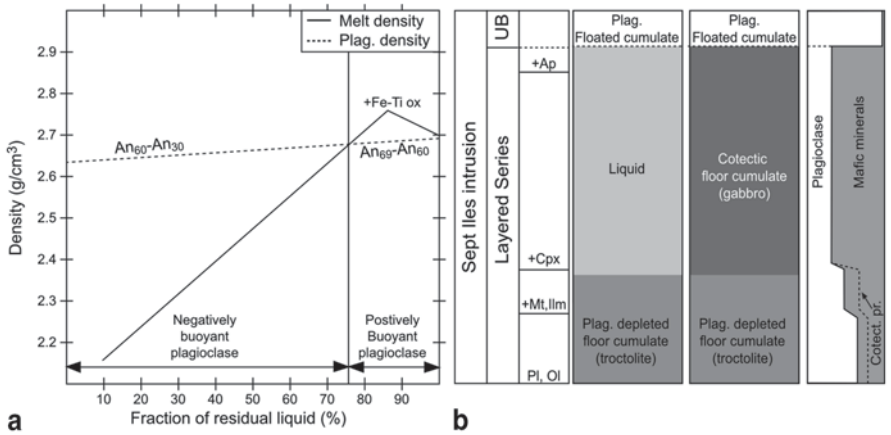

Fig. 11.18 Schematic models for the distribution of plagioclase in the Sept Iles layered intrusion (modified from Namur et al. 2011a). **a** Evolution of plagioclase and melt densities as a function of the proportion of residual liquid. Note the crossover between liquid and plagioclase density just after the saturation of Fe–Ti oxides (F = 0.76). At a higher residual melt fraction, plagioclase is positively buoyant in the basaltic melt whereas it becomes negatively buoyant when F < 0.76. **b** Simplified stratigraphic column of the Sept Iles layered intrusion showing the sequence of cumulus phases, the mechanisms of crystallization and the relative proportions of plagioclase and mafic minerals. Troctolite and Fe–Ti oxide-bearing troctolite crystallize *in situ* on the floor of the magma chamber. Plagioclase (An_{69-60}) is positively buoyant and some of the plagioclase crystals float to the top of the magma chamber where they accumulate to form a 100–500 m-thick anorthosite (Upper Border Series). After the saturation of Fe–Ti oxides (F = 0.76), the density of the magma becomes lower than that of equilibrium plagioclase (An_{60-34}), which is then no longer buoyant. Cotectic gabbro crystallizes *in situ* on the top of the previously formed troctolite crystal pile. At this stage, the anorthosite at the top of the magma chamber does not grow any further. Additional plagioclase flotation might have occurred during the crystallization of MCU III where the equilibrium liquid was locally not saturated in Fe–Ti oxides (see Fig. 11.5)

Development of Ferroan Granites

Evidence for silicic material is observed in many ferrobasaltic layered intrusions. In some cases, such as in Skaergaard, silicic rocks only form granophyre pods enclosed in the cumulates (McBirney 1989), while in other cases it forms masses of granite at the top of the intrusion (Wiebe and Snyder 1993). It has recently been suggested that the most evolved rocks of the Bushveld complex may also be of granitic composition (VanTongeren et al. 2010). Understanding the origin of these rocks is generally hampered by the lack of constraints on the ferrobasaltic liquid lines of descent in layered intrusions (Hunter and Sparks 1987; Toplis and Carroll 1996; Thy et al. 2009). The Sept Iles layered intrusion shows a clear example of ferrobasaltic layered intrusion with residual liquids evolving towards SiO_2 enrichment and FeO depletion after Fe-Ti oxide saturation. It is worth noting that the composition of Sept Iles granite is almost identical to the granophyre observed in Skaergaard and the rhyolite at the top of the Bushveld, which suggests that these two intrusions may

have followed a differentiation trend identical to that of the Sept Iles layered intrusion (Tegner and Cawthorn 2010; VanTongeren et al. 2010; Namur et al. 2011b). It is therefore important to decipher how evolved, residual liquids can be extracted from the cumulate pile and collect at the top of the magma chamber to accumulate and form granitic masses.

The history of the Sept Iles layered intrusion started with the initial filling of the magma chamber and crystallization of MCU I in the Layered Series together with the formation of the anorthositic Upper Border Series by plagioclase flotation (Namur et al. 2011a, b; Fig. 11.19a). Fractionation of troctolite and gabbro in MCU I drove the residual liquid to a monzonitic composition (e.g. 55 wt.% SiO_2; 10 wt.% FeO_t) that lay between the top of the cumulates and the bottom of the Upper Border Series (Fig. 11.19b). Using expressions from Ghiorso and Sack (1995) and Bottinga and Weill (1970), Namur et al. (2011b) estimated that the residual liquid at this stage had a temperature of ca. 1050 °C and a density of < 2.57 g/cm^3. This density is lower than that of typical anorthosite (ca. 2.70 g/cm^3; Cawthorn and Ashwal 2009; Namur et al. 2011a). Part of the residual liquid thus ascended through the partly molten anorthosite, probably helped by compaction, and accumulated at the top of the magma chamber where it formed cupolas and continued to differentiate (Fig. 11.19b). The passage of silicic liquid through the Upper Border Series anorthosite is recorded by a matrix of monzonite to syenite around plagioclase crystals and several pods and dykes of syenite within the anorthosite.

The Sept Iles layered intrusion presents two types of ferroan granite: one with magmatic mafic enclaves (MME-rich granite) and one free of enclaves. The origin of these two contrasted types of granite can be understood when magma chamber replenishments are taken into account. During the crystallization of the most evolved cumulates of MCU I (apatite-bearing gabbros), a major event of magma chamber replenishment occurred (Fig. 11.19c). Feeder dykes for this magma injection have not been clearly identified in the field, but they might be part of the same system that produced the fine- to medium-grained dykes of the Late Gabbro intrusions. Undifferentiated magma and monzonitic melts thoroughly mixed within the main magma chamber owing to vigorous convection and the highly turbulent injection. This process resulted in the formation of a very homogeneous hybrid melt (Fig. 11.19d). However, some basaltic melt reached the silicic cupolas at the top of the magma chamber (Upper Series). In these, the viscosity contrasts between basaltic and silicic melts and the absence of strong convection hampered significant mixing (Barbarin 2005). Injection of basaltic magma into the silicic magma was thus responsible for the formation of the mafic enclaves (MME) observed in one of the two granite facies form the Upper Series (Fig. 11.19d). Crystallization of MCU II also resulted in the formation of silicic melts that migrated through the anorthosite to collect at the bottom of the mostly solidified MME-bearing granite (Fig. 11.19e). Namur et al. (2011b) suggested that residual liquids from MCU II are responsible for the formation of the MME-free granite unit in the Upper Series (Fig. 11.19f). This is also in agreement with Sr isotopic ratios in cumulates from MCU II and MME-free granites.

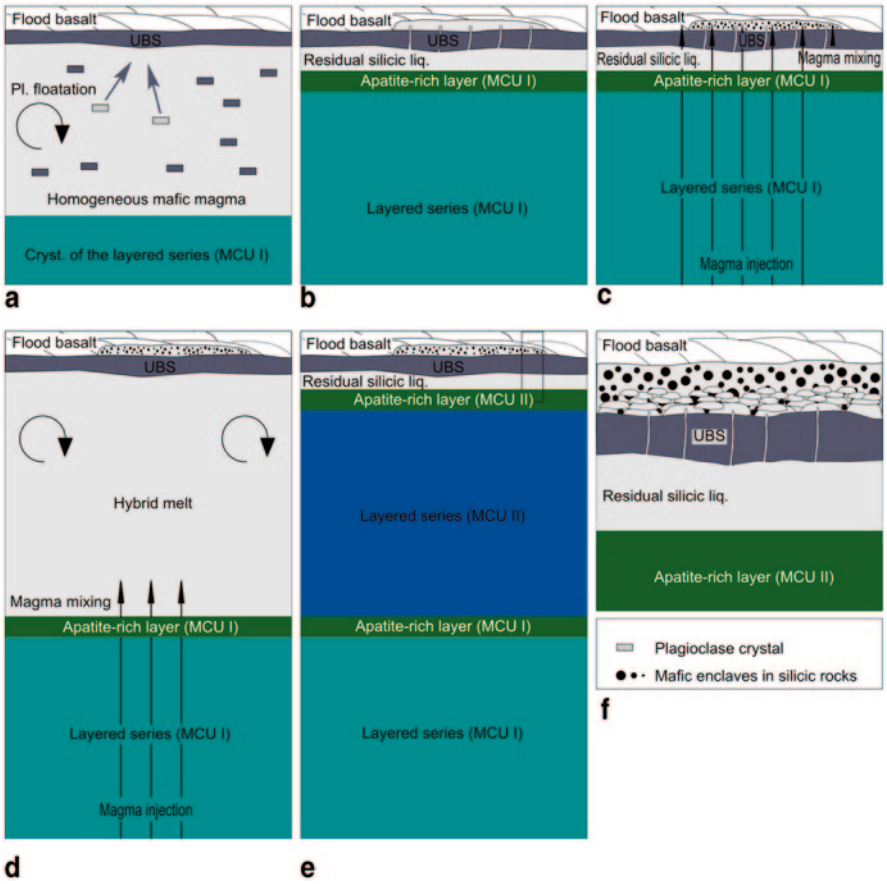

Fig. 11.19 Schematic model for the emplacement of silicic rocks in the Sept Iles layered intrusion (modified from Namur et al. 2011b). **a** Initial filling of the magma chamber and crystallization of MCU I together with simultaneous formation of the Upper Border Series (*UBS*) by plagioclase flotation (see Fig. 11.18). **b** The intermediate (monzonite) residual liquid of MCU I is less dense than the overlying anorthosite and partly ascends through the Upper Border Series to form cupolas of silicic melt at the top of the magma chamber where it further differentiates (Upper Series; *US*). **c** Magma chamber replenishment (injection of the liquid that will form MCU II) by undifferentiated magma. Complete mixing and hybridization with residual melt occurred in the main magma chamber. In contrast, mixing does not occur in silicic cupolas from the Upper Series and the injection of basalt is responsible for magma mingling and the formation of mafic enclaves (MME) in the silicic liquids of the Upper Series, forming the MME-rich granite facies (see text for details). **d** Crystallization of MCU II from a homogenous melt and differentiation of residual liquids towards SiO_2-enrichment. **e** Due to its low density, part of the residual intermediate liquids of MCU II (remaining after the crystallization of apatite-bearing olivine gabbros) ascends through the Upper Border Series. **f** These silicic liquids stay at the base of the MME-bearing silicic rocks and form the MME-free silicic rock unit of the Upper Series

Observations from the Sept Iles layered intrusion allow us to suggest that the formation of large volume of A-type granite at the top of a layered intrusion first requires a liquid line of descent evolving towards granitic composition but is

helped by the presence of rocks with high permeability, such as a loose plagioclase flotation cumulate, at the top of the magma chamber. These rocks can act as pathways for residual, low-density liquids. Migration of liquid through the anorthosite probably resulted in a channelization of the liquid which was finally collected as a series of small, km-scale, cupolas at the roof of the magma chamber. In some cases, residual silicic liquids may also be erupted from the magma chamber and form rhyolitic deposits (VanTongeren et al. 2010). In the case of the Skaergaard intrusion, the residual liquid of the Layered Series may have been extracted from the Layered Series and have contributed to increase the proportion of intercumulus melt in cumulates from the Upper Border Series, which would explain the strong enrichment in incompatible elements in these rocks (Salmonsen and Tegner 2013).

Crystal Mush Processes and Interstitial Liquid Migration

Cumulates in layered intrusions span the range from orthocumulates with more than 30 % of crystallized interstitial melt to adcumulates with virtually no crystallized interstitial melt. Experiments and theoretical modelling have shown that cumulate rocks have an initial porosity of 40–60 % (Jerram et al. 1996; Philpotts et al. 1998). Some processes must therefore occur to expel part or all the interstitial liquid from the crystal matrix during solidification. For the Skaergaard intrusion, it was suggested that these processes could be gravity-driven compaction of the crystal mush or compositional convection (Toplis et al. 2008; Tegner et al. 2009; McKenzie 2011).

Using bulk-rock compositions and plagioclase compositional profiles from the Sept Iles MCU I of the Layered Series, Namur and Charlier (2012) have shown that these two processes are not mutually exclusive and can occur together within the same intrusion. They however observed that their relative efficiency changed with differentiation. In troctolites (po-C) with plagioclase and olivine, the fraction of interstitial liquid (e.g. 30 %) is high when calculated using elements compatible in clinopyroxene and Fe–Ti oxides (Zr, Cr and V) whereas it is much lower (0–10 %) when calculated using P which is only compatible in apatite (Fig. 11.20). These results were used to suggest that the porosity in troctolites was initially reduced to ca. 30 % by compaction. This process then stops presumably due to the low-density contrast between the crystal matrix and the equilibrium ferrobasalt and the thin crystal mush at the bottom of the intrusion (Holness et al. 2007). Further porosity reduction resulted from crystallization together with compositional convection. Saturation of intercumulus Fe–Ti oxides at the bottom of the troctolite crystal mush changed the density evolution of interstitial melt from a trend of increasing density to a trend of decreasing density. Crystallization of Fe–Ti oxides therefore results in an unstable density distribution between the Fe–Ti oxide saturated interstitial melt at the bottom of the mush and interstitial melt at the top of the mush which is not yet saturated in Fe–Ti oxides (Tait et al. 1984; Toplis et al. 2008). This initiated the onset of compositional convection. Compositional convection in troctolites is

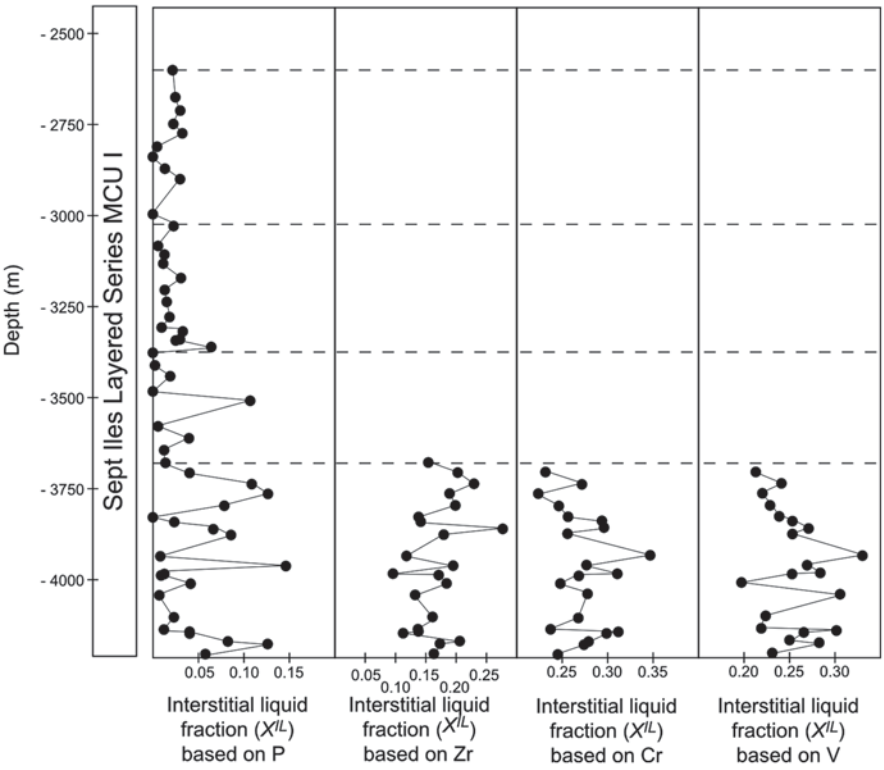

Fig. 11.20 Calculated fractions of crystallized interstitial liquid in troctolites and gabbros of the Layered Series MCU I (see Namur and Charlier 2012 for details of the calculation procedure). **a** Fraction of liquid calculated from the whole-rock and liquid P-contents. **b** Fraction of liquid calculated using Zr. **c** Fraction of liquid calculated using Cr. **d** Fraction of liquid calculated using V. Note that the liquid fractions in the po-C unit as calculated with elements of contrasting compatibilities in Sept Iles cumulus phases are quite different. Liquid fractions calculated with elements entering the structure of Fe–Ti oxides (Cr, V and Zr) are relatively high (0.15–0.40), while the liquid fractions calculated with P are very low (generally less than 0.10)

moreover revealed by plagioclase profiles with large external rims buffered to a composition of An_{61}, similar to those observed in Skaergaard and interpreted as forming during solidification of interstitial melt buffered at a constant composition due to liquid convection through the mush (Toplis et al. 2008).

In gabbros with cumulus Fe–Ti oxides, compositional convection and compaction are probably both efficient in expelling (or exchanging) melt from the crystal mush. The distribution of the last fraction of intercumulus melt in Sept Iles cumulates, as recorded by the whole-rock P content, is significantly different in troctolites (po-C) and Fe–Ti oxide-bearing rocks (pomi-C to pmic-C). In troctolites, the distribution of P is heterogeneous, and high and low values alternate at a scale of 30–250 m. In Fe–Ti oxide-bearing rocks, the distribution of the whole-rock P content is less variable, suggesting that the last fraction of intercumulus

melt was homogeneously distributed within the mush. Namur and Charlier (2012) used this information to suggest that expulsion of interstitial liquid from Fe–Ti oxide-bearing cumulates is dominated by compaction, resulting in a porous flow, rather than compositional convection which may produce highly-channelized flow (Worster 1992) and which is therefore more likely to produce a heterogeneous distribution of the liquid within the crystal mush. The role of compaction in Fe–Ti oxide-bearing rocks is moreover illustrated by the high aspect-ratio of their plagioclase crystals and the development of well-defined mineral lamination (Namur and Charlier 2012).

Formation of Fe–Ti–P Ore Deposits

Two 200 m-thick sequences of apatite-bearing gabbro occur at the top of MCU I and MCU II. These sequences are significantly enriched in P, Fe and Ti. The uppermost level was drilled by the Soquem Inc in the 1990s and more than 30 cores, up to 250 m long, were retrieved along a 7 km long east-west traverse on the mainland. Apatite-bearing gabbros are the most evolved cumulates of MCU I and MCU II. In MCU I, they are homogeneous leucocratic gabbros with 3–4 vol.% apatite and 15–20 vol.% Fe–Ti oxides. In MCU II, they show an alternation on a 5–20 m scale between leucocratic gabbros (<5 vol.% apatite; <10 vol.% Fe–Ti oxides) and melanocratic gabbros (up to 25 vol.% apatite and 60 vol.% Fe–Ti oxides). Based on an incremental forward model of crystallization, it has been shown that the liquid lines of descent for MCU I and MCU II are slightly different for all the major elements (Namur et al. 2012a). This is related to the extent of magma mixing during the important replenishment event that initiated the crystallization of MCU II as well as minor replenishments that took place during its formation. Minor compositional differences can have important consequences for the physical and chemical evolution of the liquid as well as for the formation of cumulates. When liquid lines of descent for MCU I and MCU II are plotted in the ternary diagram Si–Al–Ca (Charlier and Grove 2012), it emerges that the bulk liquids of MCU II entered a two-liquid field and that immiscibility developed (Fig. 11.21). Immiscibility during crystallization of MCU II is shown by contrasting Fe-rich and Si-rich apatite-hosted melt inclusions (Charlier et al. 2011). In contrast, liquids formed during the crystallization of MCU I never encountered the two-liquid compositional field (Fig. 11.21). Crystallization from a homogeneous magma in MCU I resulted in the formation of homogeneous leucocratic apatite-bearing gabbros. In MCU II, Fe-rich and Si-rich immiscible liquids were segregated on a 5–20 m scale, although chemical equilibrium between both liquids was probably maintained. Whether the whole magma body reached immiscibility at the same time or immiscibility occurred repeatedly in basal layers at the top of the crystal pile is not known (Charlier et al. 2011). It is however suggested that crystallization from the two immiscible liquids resulted in the formation of alternating highly leucocratic gabbro and highly melanocratic gabbro (Charlier et al. 2011; Namur et al. 2012a).

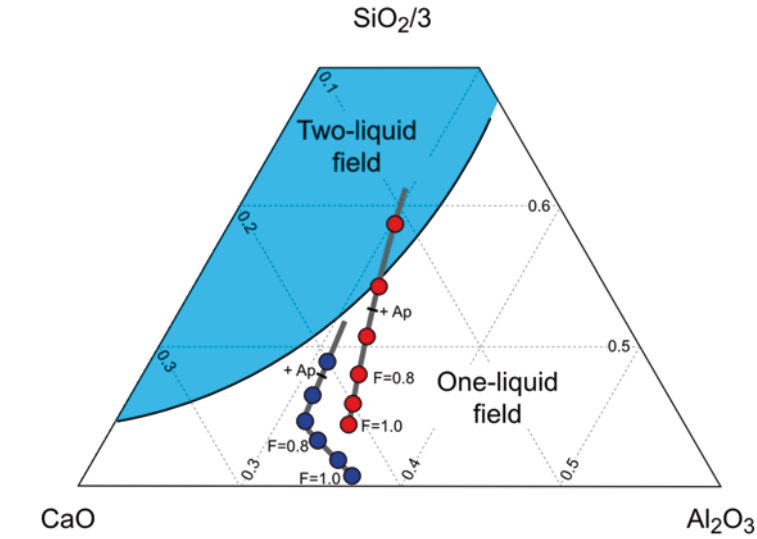

Fig. 11.21 Representation of liquid lines of descent for MCU I (*blue circles*) and MCU II (*red circles*) in a subsection of the SiO_2–CaO–Al_2O_3 compositional space. The positions of the one-liquid field (*white*), two-liquid field (*blue*) and the binodal are from Charlier and Grove (2012). *F* fraction of residual liquid; *+Ap* the initiation of apatite crystallization. Distance between each circle corresponds to 10 % of fractional crystallization. Incremental forward models stop at F = 0.45. Note that the residual liquids from MCU I do not encounter the two-liquid field unlike those from MCU II

Large-scale segregation of immiscible melts, as opposed to simple fractional crystallization of a homogeneous melt, is proposed as a very efficient process to concentrate economically important minerals such as apatite, magnetite and ilmenite in layered intrusions. Nevertheless, some more work is needed to understand how the immiscible liquids actually segregated (Chung and Mungall 2009) and were stratigraphically organized within the magma chamber.

Conclusions

The Sept Iles Intrusive Suite is made up of three igneous units, of which the layered intrusion is by far the most voluminous. The other units are late-stage gabbro intrusions and the Pointe du Criard composite sill. The cumulates in the layered intrusion crystallized from a ferrobasaltic parent magma and form a succession with the following sequence of crystallization: plagioclase and olivine, followed by Fe–Ti oxides, then clinopyroxene and finally apatite. This order of crystallization was interrupted by several replenishments of the magma chamber and the Layered Series can be subdivided into three megacyclic units (MCUs), each of them having crystallized

similar sequences of cumulates. Magma chamber replenishments produced lateral and vertical extension of the magma chamber and therefore significantly enlarged its size compared to the initial magma chamber.

Saturation of Fe–Ti oxides in the Layered Series changed the evolution of melt density from a trend of increasing density to one of decreasing density. Before Fe–Ti oxide saturation, some plagioclase crystals that nucleated and grew at the floor of the magma chamber floated to the roof of the chamber, where they accumulated to produce the anorthosite of the Upper Border Series. Appearance of cumulus Fe–Ti oxides and the resulting decrease in magma density prevented plagioclase grains from further floating and cotectic cumulate rocks started to crystallize at the base of the magma chamber. Eventually, altered blocks of anorthosite fell from the roof to the top of the crystal pile and were buried as autoliths within the Layered Series. The evolution of liquid density associated with the saturation of Fe–Ti oxides has also implications for the evolution of the interstitial melt within the solidifying crystal mushes at the floor of the magma chamber. Appearance of liquidus Fe–Ti oxides is thought to have changed the main way the interstitial melt was expelled from compositional convection in troctolites to cumulate compaction in Fe–Ti oxide-bearing gabbros.

Fractionation of cumulates forming the Sept Iles Layered Series from the ferrobasaltic parent magma resulted in a liquid line of descent towards SiO_2 enrichment and FeO depletion after the saturation of Fe–Ti oxides. This liquid line of descent had a limited proportion of intermediate melts (e.g. 57–67 wt.% SiO_2). Minor country-rock assimilation took place concurrently with differentiation but did not play an important role in the geochemical evolution of Sept Iles liquids. SiO_2 enrichment during crystallization had important implications for the dynamic evolution of the magma chamber. Residual liquids produced during the crystallization of MCU II encountered a two-liquid immiscibility field. This produced contrasting Si-rich and Fe-rich immiscible melts and hence accounts for the absence of intermediate liquid compositions. On the other hand, residual liquids from MCU I never reached the two-liquid field. The limited proportion of intermediate liquids observed along the Sept Iles liquid line of descent is therefore related only to the differentiation of MCU I. The onset of immiscibility in MCU II also resulted in the crystallization of cumulate rocks from contrasting and spatially segregated immiscible melts. This produced alternating sequences of leucocratic and melanocratic apatite-bearing gabbros towards the top of MCU II. Immiscibility is proposed as an efficient process for the concentration of mafic minerals and apatite, and the production of Fe–Ti–P mineralization in layered intrusions (Namur et al. 2015; Veksler and Charlier 2015). In MCU I, fractional crystallization of a single homogeneous liquid also led to the crystallization of apatite-bearing gabbros, but these are comparatively leucocratic and are currently of no economic interest.

Acknowledgements Research on Sept Iles by the authors was funded by the Belgian National Fund for Scientific Research (FNRS), the Belgian Fund for Research in Industry and Agriculture (FRIA) and the Natural Science and Engineering Research Council of Canada, Discovery grants program. ON acknowledges the FRIA for a position as PhD student and the University of Liège for a teaching assistantship. ON also acknowledges support from the Natural Environment

Research Council (NERC; United Kingdom), Newton Trust and Magdalene College (University of Cambridge). The Ministère des Ressources Naturelles et de la Faune du Québec and Soquem Inc are thanked for access to drill-cores. We would to thank B. Charlier, J.C. Duchesne, M.J. Toplis, J.P. Liégeois, J. Hermann, C. Pirard and M.B. Holness for comments. Analytical support by G. Bologne, N. Delmelle, H.J. Bernhardt, C. Gilson, C. Allen and J.L. Devidal was also highly appreciated. Constructive reviews by B. Robins and J. VanTongeren as well as detailed comments and editorial handling by R. Latypov were highly appreciated and significantly improved the quality of the manuscript.

References

Barbarin B (2005) Mafic magmatic enclaves and mafic rocks associated with some granitoids of the central Sierra Nevada batholith, California: nature, origin, and relations with the hosts. Lithos 80:155–177

Beard JS, Lofgren GE (1991) Dehydration melting and water-saturated melting of basaltic and andesitic greenstones and amphibolites at 1, 3 and 6.9 kbar. J Petrol 32:365–401

Bonin B (2007) A-type granites and related rocks: evolution of a concept, problems and prospects. Lithos 97:1–29

Botcharnikov RE, Almeev RR, Koepke J, Holtz F (2008) Phase relations and liquid lines of descent in hydrous ferrobasalt: implications for the Skaergaard intrusion and Columbia river flood basalts. J Petrol 49:1687–1727

Bottinga Y, Weill DF (1970) Densities of liquid silicate systems calculated from partial molar volumes of oxide components. Am J Sci 269:169–182

Brandeis G, Jaupart C (1986) On the interaction between convection and crystallization in cooling magma chambers. Earth Planet Sci Lett 77:345–361

Campbell IH, Turner JS (1986) The influence of viscosity on fountains in magma chambers. J Petrol 27:1–30

Campbell IH, Turner JS (1989) Fountains in magma chambers. J Petrol 30:885–923

Carmichael IS (1964) The petrology of Thingmuli, a tertiary volcano in Eastern Iceland. J Petrol 5:435–460

Cawthorn RG (2012) Multiple sills or a layered intrusion: time to decide. S Afr J Geol 115:283–290

Cawthorn RG, Ashwal LD (2009) Origin of anorthosite and magnetitite layers in the Bushveld complex, constrained by major element compositions of plagioclase. J Petrol 50:1607–1637

Charlier B, Grove TL (2012) Experiments on liquid immiscibility along tholeiitic liquid lines of descent. Contrib Mineral Petrol 164:27–44

Charlier B, Namur O, Toplis MJ, Schiano P, Cluzel N, Higgins MD, Vander Auwera J (2011) Large-scale silicate liquid immiscibility during differentiation of tholeiitic basalt to granite and the origin of the daly gap. Geology 39:907–910

Charlier B, Namur O, Grove TL (2013) Compositional and kinetic controls on liquid immiscibility in ferrobasalt-rhyolite volcanic and plutonic series. Geochim Cosmochim Acta 113:79–93

Charreteur G, Tegner C (2013) Multiple ways of producing intermediate and silicic rocks within Thingmúli and other Icelandic volcanoes. Contrib Mineral Petrol 166:471–490

Cheney E S, Twist D (1991) The conformable emplacement of the Bushveld mafic rocks along a regional unconformity in the Transvaal succession of South Africa. Precambrian Res 52:115–132

Chung HY, Mungall JE (2009) Physical constraints on the migration of immiscible fluids through partially molten silicates, with special reference to magmatic sulfide ores. Earth Planet Sci Lett 286:14–22

Cimon J (1998) Le Complexe de Sept-Îles: I – L'Unité à apatite de Rivière des Rapides, Complexe de Sept-Îles; localisation stratigraphique et facteurs à l'origine de sa formation. ET 97–05, Ministère de l'Énergie et des Ressources du Québec, 1:1–33

Clemens JD, Holloway JR, White RJ (1986) Origin of an A-type granite: experimental constraints. Am Mineral 71:317–324
Danyushevsky L, Perfit M, Eggins S, Falloon T (2003) Crustal origin for coupled ultra-depleted and plagioclase signatures in MORB olivine-hosted melt inclusions: evidence from the Siqueiros Transform Fault, East Pacific Rise. Contrib Mineral Petrol 144:619–637
DePaolo DJ (1981) Trace element and isotopic effects of combined wallrock assimilation and fractional crystallization. Earth Planet Sci Lett 53:189–202
Doig R (1970) An alkaline rock province linking Europe and North America. Can J Earth Sci 7:22–28
Doig R, Barton JM (1968) Ages of carbonatites and other alkaline rocks in Quebec. Can J Earth Sci 5:1401–1407
Duchesne JC, Bologne G (2009). XRF major and trace element determination in Fe–Ti oxide minerals. Geol Belg 12:205–212
Eby GN (1990) The A-type granitoids: a review of their occurrence and chemical characteristics and speculations on their petrogenesis. Lithos 26:115–134
Egorova V, Latypov R (2012) Prolonged magma emplacement as a mechanism for the origin of the marginal reversal of the Fongen–Hyllingen layered intrusion, Norway. Geol Mag 149:909–926
Falloon T, Green D, Danyushevsky L, Faul U (1999) Peridotite melting at 1.0 and 1.5 GPa: An experimental evaluation of techniques using diamond aggregates and mineral mixes for determination of near-solidus melts. J Petrol 40:1343–1375
Frost BR, Barnes CG, Collins WJ, Arculus RJ, Ellis DJ, Frost CD (2001) A geochemical classification for granitic rocks. J Petrol 42:2033–2048
Ghiorso MS, Sack RO (1995) Chemical mass transfer in magmatic processes IV. A revised and internally consistent thermodynamic model for the interpolation and extrapolation of liquid-solid equilibria in magmatic systems at elevated temperatures and pressures. Contrib Mineral Petrol 119:197–212
Grove TL, Donnelly-Nolan JM (1986) The evolution of young silicic lavas at Medicine Lake Volcano, California: implications for the origin of compositional gaps in calc-alkaline series lavas. Contrib Mineral Petrol 92:281–302
Higgins MD (1990) A three-component composite dyke and its associated intrusion, the Pointe du Criard, Quebec, Canada. In: Parker A, Rickwood P, Tucker D (eds) Mafic dykes and emplacement mechanism. Balkema, Rotterdam, pp 63–68
Higgins MD (1991) The origin of laminated and massive anorthosite, Sept Iles layered intrusion, Quebec, Canada. Contrib Mineral Petrol 106:340–354
Higgins MD (2005) A new interpretation of the structure of the Sept Iles Intrusive Suite, Canada. Lithos 83:199–213
Higgins MD (2011) Textural coarsening in igneous rocks. Int Geol Rev 53:354–376
Higgins MD, Chandrasekharam D (2007) Nature of sub-volcanic magma chambers, Deccan Province, India: evidence from quantitative textural analysis of plagioclase megacrysts in the giant plagioclase Basalts. J Petrol 48:885–900
Higgins MD, Doig R (1977) 540-Myr-old anorthosite complex in the Grenville Province of Quebec, Canada. Nature 267:40–41
Higgins MD, Doig R (1981) The Sept Iles anorthosite complex: field relationships, geochronology, and petrology. Can J Earth Sci 18:561–573
Higgins MD, Doig R (1986) Geochemical constraints on the differentiation processes that were active in the Sept Iles complex. Can J Earth Sci 23:670–681
Higgins MD, van Breemen O (1998) The age of the Sept Iles layered mafic intrusion, Canada: implications for the late Neoproterozoic/Cambrian history of southeastern Canada. J Geol 106:421–432
Hill RI, Campbell IH, Davies G, Griffiths RW (1992) Mantle plumes and continental tectonics. Science 256:186–193
Holness MB, Vernon RH (2015) The influence of interfacial energies on igneous microstructures. In: Charlier et al. (eds) Layered Intrusions, Springer Geology

Holness MB, Tegner C, Nielsen TFD, Stripp G, Morse SA (2007) A textural record of solidification and cooling in the Skaergaard intrusion, East Greenland. J Petrol 48:2359–2377
Hoover JD (1989) The chilled marginal gabbro and other contact rocks of the Skaergaard intrusion. J Petrol 30:441–476
Hounsell V (2006) Origine des roches felsiques de la serie superieure de la suite intrusive de Sept-Iles, Quebec. Master's thesis, University of Quebec in Chicoutimi (UQAC)
Hunter RH, Sparks RS (1987) The differentiation of the Skaergaard intrusion. Contrib Mineral Petrol 95:451–461
Irvine TN (1982) Terminology for layered intrusions. J Petrol 23:127–162
Irvine TN, Baragar WR (1971) A guide to chemical classification of common volcanic rocks. Can J Earth Sci 8:315–341
Irvine TN, Andersen JC, Brooks CK (1998) Included blocks (and blocks within blocks) in the Skaergaard intrusion: geologic relations and the origins of rhythmic modally graded layers. Geol Soc Am Bull 110:1398–1447
Jerram D, Cheadle M, Hunter R, Elliott M. (1996) The spatial distribution of grains and crystals in rocks. Contrib Mineral Petrol 125:60–74
Juster T, Grove TL, Perfit M (1989) Experimental constraints on the generation of FeTi basalts, andesites, and rhyodacites at the Galapagos Spreading Center, 85 W and 95 W. J Geophys Res 94:9251–9274
Kamo SL, Gower CF, Krogh TE (1989) Birthdate for the Iapetus Ocean? A precise U–Pb zircon and baddeleyite age for the Lang Range Dykes, southeast Labrador. Geology 17:602–605
Kruger FJ (2005) Filling the Bushveld Complex magma chamber: lateral expansion, roof and floor interaction, magmatic unconformities, and the formation of giant chromitite, PGE and T-V-magnetitite deposits. Miner Deposita 40:451–472
Kumarapeli PS (1993) A plume-related segment in the rifted margin of Laurentia, southern Canadian Appalachians, seen through a completed Wilson cycle. Tectonophysics 219:47–55
Kumarapeli PS, Saull VA (1966) The St Lawrence valley system: a north American equivalent to the East African rift valley system. Can J Earth Sci 3:639–658
Lajeunesse, P. St-Onge, G. Locat, J., Duchesne, M.J., Higgins, M.D., Sanfacon, R., Ortiz, J. (2013). The Corossol structure: A possible crater on the seafloor of the northwestern gulf of St. Lawrence, Eastern Canada. Meteor Planet Sci 48:2542–2558
Latypov R, Hanski E, Lavrenchuk A, Huhma H, Havela T (2011) A 'three-increase model' for the origin of the marginal reversal of the Koitelainen layered intrusion, Finland. J Petrol 52:733–764
Lightfoot PC, Hawkesworth CJ, Sethna SF (1987) Petrogenesis of rhyolites and trachyes from the Deccan trap: Sr, Nd and Pb isotope and trace element evidence. Contrib Mineral Petrol 95:44–54
Loiselle MC, Wones D (1979) Characteristics and origin of anorogenic granites. Geol Soc Am, Abstracts with Program. 11, 468
Loncarevic BD, Feininger T, Lefebvre D (1990) The Sept-Iles layered mafic intrusion: geophysical expression. Can J Earth Sci 27:501–512
McBirney AR (1989) The Skaergaard Layered Series: I. structure and average compositions. J Petrol 30:363–397
McBirney AR, Naslund HR (1990) The differentiation of the Skaergaard intrusion: A discussion of Hunter and Sparks. Contrib Mineral Petrol 104:235–240
McKenzie D (2011) Compaction and crystallization in magma chambers: towards a model for the Skaergaard intrusion. J Petrol 52:905–930
Morse SA (1990) The differentiation of the Skaergaard intrusion: a discussion of Hunter and Sparks. Contrib Mineral Petrol 104:240–244
Namur O, Charlier B (2012) Efficiency of compaction and compositional convection during mafic crystal mush solidification: the Sept Iles layered intrusion, Canada. Contrib Mineral Petrol 163:1049–1068

Namur O, Charlier B, Toplis MJ, Higgins MD, Liegeois JP, Vander Auwera J (2010) Crystallization sequence and magma chamber processes in the ferrobasaltic Sept Iles Layered Intrusion, Canada. J Petrol 51:1203–1236

Namur O, Charlier B, Pirard C, Hermann J, Liegeois JP, Vander Auwera J (2011a) Anorthosite formation by plagioclase flotation in ferrobasalt and implications for the lunar crust. Geochim Cosmochim Acta 75:4998–5018

Namur O, Charlier B, Toplis MJ, Higgins MD, Hounsell V, Liegeois JP, Vander Auwera J (2011b) Differentiation of tholeiitic basalt to A-type granite in the Sept Iles Layered Intrusion, Canada. J Petrol 52:487–539

Namur O, Charlier B, Holness MB (2012a) Dual origin of Fe–Ti–P gabbros by immiscibility and fractional crystallization of evolved tholeiitic basalts in the Sept Iles layered intrusion. Lithos 154:100–114

Namur O, Charlier B, Toplis MJ, Vander Auwera J (2012b) Prediction of plagioclase-melt equilibria in anhydrous silicate melts at 1-atm. Contrib Mineral Petrol 163:133–150

Namur O, Abily B, Boudreau A, Blanchette F, Bush JWM, Ceuleneer G, Charlier B, Donaldson CH, Duchesne JC, Higgins MD, Morata D, Nielsen TFD, O'Driscoll B, Pang KW, Peacock T, Spandler C, Toramaru A, Veksler I (2015) Igneous layering in basaltic magma chambers. In: Charlier et al. (eds) Layered Intrusions, Springer Geology

Niu Y, Batiza R (1991) In situ densities of MORB melts and residual mantle: implications for buoyancy forces beneath mid-ocean ridges. J Geol 99:767–775

Panjasawatwong Y, Danyushevsky LV, Crawford AJ, Harris KL (1995) An experimental study of the effects of melt composition on plagioclase-melt equilibria at 5 and 10 kbar: implications for the origin of magmatic high-An plagioclase. Contrib Mineral Petrol 118:420–432

Patino Douce AE (1997) Generation of metaluminous A-type granites by low-pressure melting of calc-alkaline granitoids. Geology 25:743–746

Peccerillo A, Barberio MR, Yirgu G, Ayalew D, Barbieri M, Wu TW (2003) Relationships between Mafic and Peralkaline silicic magmatism in continental rift settings: a petrological, geochemical and isotopic study of the gedemsa volcano, central Ethiopian rift. J Petrol 44:2003–2032

Philpotts AR, Carroll M (1996) Physical properties of melted tholeiitic basalt. Geology 24:1029–1032

Philpotts AR, Shi J, Brustman C (1998) Role of plagioclase crystal chains in the differentiation of partly crystallized basaltic magma. Nature 395:343–346

Rivers T (2008) Assembly and preservation of lower, mid, and upper orogenic crust in the Grenville Province: Implications for the evolution of large hot long-duration orogens. Precambrian Res 167:237–259

Rivers T, Martignole J, Gower CF, Davidson A (1989) New tectonic divisions of the Grenville Province, southeastern Canadian shield. Tectonics 8:63–84

Roelofse F, Ashwal LD (2012) The lower and main zone in the northern limb of the bushveld complex: a 1.3 km thick sequence of intruded and variably contaminated crystal mushes. J Petrol 53:1449–1476

Salmonsen L, Tegner C (2013) Crystallization sequence of the Upper Border Series of the Skaergaard Intrusion: revised subdivision and implications for chamber-scale magma homogeneity. Contrib Mineral Petrol 165:1155–1171

Snyder D, Carmichael IS, Wiebe RA (1993) Experimental study of liquid evolution in an Fe-rich, layered mafic intrusion: constraints of Fe–Ti oxide precipitation on the T-fO2 and T-p paths of tholeiitic magmas. Contrib Mineral Petrol 113:73–86

Tait S, Huppert HE, Sparks RS (1984) The role of conpositional convection in the formation of adcumulate rocks. Lithos 17:139–146

Tegner C (1997) Iron in plagioclase as a monitor of the differentiation of the Skaergaard intrusion. Contrib Mineral Petrol 128:45–51

Tegner C, Cawthorn RG (2010) Iron in plagioclase in the Bushveld and Skaergaard intrusions: implications for iron contents in evolving basic magmas. Contrib Mineral Petrol 159:719–730

Tegner C, Wilson JR, Robins B (2005) Crustal assimilation in basalt and jotunite: constraints from layered intrusions. Lithos 83:299–316

Tegner C, Cawthorn RG, Kruger FJ (2006) Cyclicity in the main and upper zones of the Bushveld complex, South Africa: crystallization from a zoned magma sheet. J Petrol 47:2257–2279
Tegner C, Thy P, Holness MB, Jakobsen JK, Lesher CE (2009) Differentiation and compaction in the Skaergaard intrusion. J Petrol 50:813–840
Thy P, Lesher CE, Tegner C (2009) The Skaergaard liquid line of descent revisited. Contrib Mineral Petrol 157:735–747
Toplis MJ (2005) The thermodynamics of iron and magnesium partitioning between olivine and liquid: criteria for assessing and predicting equilibrium in natural and experimental systems. Contrib Mineral Petrol 149:22–39
Toplis MJ, Carroll M (1995) An experimental study of the influence of oxygen fugacity on Fe–Ti oxide stability, phase relations, and mineral-melt equilibria in ferro-basaltic systems. J Petrol 36:137–1170
Toplis MJ, Carroll MR (1996) Differentiation of ferro-basaltic magmas under conditions open and closed to oxygen: implications for the Skaergaard intrusion and other natural systems. J Petrol 37:837–858
Toplis MJ, Brown W, Pupier E (2008) Plagioclase in the Skaergaard intrusion. Part 1: core and rim compositions in the layered series. Contrib Mineral Petrol 155:329–340
VanTongeren J, Mathez E, Kelemen P (2010) A felsic end to Bushveld differentiation. J Petrol 51:1891–1912
Veksler IV, Charlier B (2015) Silicate liquid immiscibility in layered intrusions. In: Charlier et al. (eds) Layered Intrusions, Springer Geology
Wager LR, Brown GM (1968) Layered igneous rocks. Oliver & Boyd, Edinburgh
Wiebe RA, Snyder D (1993) Slow, dense replenishments of a basic magma chamber: the layered series of the Newark Island layered intrusion, Nain, Labrador. Contrib Mineral Petrol 113:59–72
Wilson JR, Larsen SB (1982) Discordant layering relations in the Fongen–Hyllingen basic intrusion. Nature 299:625–626
Wilson JR, Robins B, Nielsen FM, Duchesne JC, Vander Auwera J (1996) The Bjerkreim–Sokndal layered intrusion, Southwest Norway. In Cawthorn RG (ed) Layered intrusions. Elsevier, Amsterdam
Worster M (1992) Instabilities of the liquid and mushy regions during solidification of alloys. J Fluid Mech 237:649–669